ABSTRACT

Title of Document: NOVEL METHODOLOGY FOR CALCIUM MEASUREMENTS IN CONSCIOUS MICE: AN APPLICATION TO ARTERIOLAR VASOMOTION

Adam Lyle Zviman, Master of Science, 2015

Directed By: Dr. Withrow Gil Wier, Department of Physiology, University of Maryland, Baltimore

We developed a method employing two-photon microscopy and genetically engineered 'Ca^{2+}- biosensor' mice to measure Ca^{2+} signaling in arteries of conscious, head-fixed mice. Arterial blood pressure was measured simultaneously via implanted telemetric pressure transducers. These methods allowed, for the first time, the study of control of arterial [Ca^{2+}], diameter, and blood pressure by sympathetic nerve activity (SNA) as it normally exists in conscious animals. We tested the hypothesis that arterial vasomotion, observed more frequently in conscious animals than in anesthetized animals, was generated by SNA that caused synchronous Ca^{2+}-oscillations in smooth muscle. We also measured the changes in arterial [Ca^{2+}] that occur during the time course of experimental hypertension. Pharmacological block of SNA and isoflurane anesthesia eliminated and attenuated, respectively, vasomotion and reduced arterial [Ca^{2+}] (320 ± 48 nM to 241 ± 20 nM and 302 ± 48 nM). This method allows for longitudinal studies of important chronic vascular pathologies.

NOVEL METHODOLOGY FOR CALCIUM MEASUREMENTS IN CONSCIOUS MICE: AN APPLICATION TO ARTERIOLAR VASOMOTION

By

Adam Lyle Zviman

Thesis submitted to the Faculty of the Graduate School of the
University of Maryland, College Park, in partial fulfillment
of the requirements for the degree of
Master of Science
2015

Advisory Committee:
Professor Withrow Gil Wier, Co-Chair
Dr. Yu Chen, Co-Chair
Dr. Steven Jay

Dedication

To my parents, Denise and Muz, for unwavering support and love during my two decade-long academic career. I love you two very much.

To Alex, for all the "gimmes" and laughs we shared over the course of the year. Without you, I surely would have lost my way. I'm looking forward to sharing in this accomplishment with you.

To Skott, who is undoubtedly the best roommate and brother ever to exist. Not too shabby at goalkeeper, either. Thanks for saving me from the pool pizza delivery disaster of the early 1990s.

To Jen, Matt, and the little ones, who have always supported me through thick and thin. Much love.

Acknowledgements

I'd like to give my thanks to various people that have guided me throughout this process:

First and foremost, to Dr. Gil Wier, for teaching me so much about research and cardiovascular physiology (both directly and indirectly). I must also thank you for the advice you gave me in so many topics, from career decisions to personal finance to experimental design. Thanks so much for giving me such an amazing opportunity and taking me on in the lab. I had a great time learning from you.

To Dr. Joe Mauban, for helping me get the project off the ground and helping me with all the practical stuff. Also, thank you for keeping the atmosphere "JOEvial" (read: jovial) in otherwise trying and frustrating times. Joe, you are truly the jack-of-all-trades.

To (future Dr.) Scarlett Hao, for teaching me surgical techniques and practical mouse handling knowledge. I'm looking forward to being on the wards together!

To Dr. Seth Fairfax for his help in getting started with the hypertension study. To Michele Markwardt, for purifying and characterizing the proteins I used for the study (and excellent Game of Thrones gossip). To Dr. Jin Zhang and Dr. Youhua Wang for help in setting up the troublesome calibration experiments. To Dr. Ling Chen and Dr. Laureano Asico for their help in installation of blood pressure transducers.

Table of Contents

List of Figures

Chapter 1: Introduction

1.1) Motivation

Cardiovascular physiology has historically relied upon *in vivo* studies to glean understanding of the processes that govern function. In the 1970s, Guyton and colleagues performed landmark experiments that set the basis for the field; however these early experiments were unable to shed light on molecular regulation of cardiovascular function. As molecular biology techniques (isolated cells, cell lines, tissue culture, etc…) evolved in the past half-century, focus has been put on *ex vivo* experiments that allow for the elucidation of molecular mechanisms that can be observed in the heart and vasculature. While these experiments describe what may be seen in the living animal, they do not provide a true depiction of the *in vivo* cellular environment. The implication of this is not trivial: important physiological mechanisms may have different contributions from molecular players than were determined from *ex vivo* studies.

An important example of such a discrepancy is the phenomenon of asynchronous propagating Ca^{2+} waves seen in isolated vascular segments. Much of what we know about vascular smooth muscle (VSM) function and its relationship to intracellular Ca^{2+} signaling arises from *ex vivo* experiments in which a vessel is excised and examined without influence of circulatory factors or autonomic nervous control[1]. In isolated arteries subjected to phenylephrine (an α_1-receptor agonist), asynchronous propagating Ca^{2+} waves appear readily; however, it has been observed that

asynchronous propagating Ca^{2+} waves in VSM do not occur *in vivo* [2-5]. This suggests that such Ca^{2+} signals are elementary and are not present in the intact physiological system.

Recently, improvements in imaging technology and biosensors have allowed for development of new techniques to non-invasively evaluate vascular physiology. Specifically, three developments were key to the present work: 1) refinement of genetically encoded fluorescence biosensor molecules, like the Förster resonance energy transfer (FRET)-based one used in this work, 2) two-photon imaging, which allows for non-invasive optical imaging (even within scattering tissue), and 3) implantation of telemetric blood pressure transducers that allow for evaluation of hemodynamics (and importantly, don't cause pain or discomfort to the animal). Previous work in our lab has applied these developments and quantified $[Ca^{2+}]$ within resistance blood vessels in the conscious, restrained mouse[2]. This thesis aims to expand on previous work and describe methodology to allow for $[Ca^{2+}]$ imaging and quantification in arterioles of conscious, head-fixed mice.

1.2) Vasomotion

Vasomotion, defined as the oscillatory change in diameter of blood vessels, was first described in the bat wing vasculature in in mid-19th century. Since then, there has been much work into elucidating the mechanism and physiological purpose of the phenomenon. Vasomotion occurs in most vascular beds and can exhibit a range of frequencies from 0.01 to 0.3 Hz *in vivo*[6, 7] and occurs independently of heart rate and

respiration. Oscillatory behavior of blood vessels has been appreciated in many species and across all sizes of vessel. The behavior can be elicited *in vitro* with administration of adrenergic agonists and exhibits similar frequencies to those seen *in vivo*.

Early work in characterizing the cellular basis for vasomotion has shown that coordination of intracellular Ca^{2+} concentration ($[Ca^{2+}]_i$) changes amongst VSM cells is required for vasomotion to occur[8, 9]. Interestingly, vasomotion elicited by adrenergic stimulation *ex vivo* is often preceded by asynchronous Ca^{2+} waves that propagate along the long axis of the VSM cells before synchronization of $[Ca^{2+}]_i$ and vasomotion occurs. At that time, the Ca^{2+} waves disappear and only synchronous changes in global $[Ca^{2+}]_i$ are seen[7, 8]. Rhythmical changes in smooth muscle membrane potential also occur with the phenomenon, and are necessary for the generation of global $[Ca^{2+}]$ changes (and consequent vasomotion) in arterial smooth muscle. In addition, an intact endothelium is necessary, as denuded arteries do not exhibit vasomotion without additional manipulation[10].

The physiological consequences of vasomotion are still debated, however it is postulated that the phenomenon is important for tissue dialysis and blood flow. Increased washout of a radiotracer from the interstitial compartment of the rabbit ear was noted in vessels undergoing vasomotion as compared to a static state with the same mean blood flow[11]. It has been shown that a vessel undergoing vasomotion has decreased vascular hydraulic resistance than a static vessel with the same mean

radius[12]. Mathematical modeling of vasomotion (modeled as periodic fluctuations in red blood cell velocity) has shown that vasomotion enhances O_2 delivery to tissue[13-15] whereas some studies solving the Navïer-Stokes equation using an oscillatory boundary condition have concluded that O_2 delivery via arterioles are decreased, possibly enhancing oxygen tension and delivery at the capillaries[15].

Previous study of the occurrence of vasomotion has shown that significantly more vasomotion occurs in areas threatened by metabolic stress[16, 17]. This is suggested by studies describing increased prevalence of vasomotion at the hypotensive-end of autoregulatory pressure range[18] as well as in various disease states; diabetes mellitus, hypertension, and hemorrhage have been associated with increases in incidence of vasomotion across several vascular beds[7]. Laser doppler flow (LDF) analysis of cutaneous arteries from patients with peripheral arterial occlusive disease exhibit increased vasomotion[19]. Pathological vascular changes resulting from these conditions result in impaired tissue perfusion, which may serve to initiate compensatory mechanisms, like vasomotion, to re-establish blood flow.

Increased sympathetic nerve activity (SNA) has been implicated in all of the aforementioned pathological conditions[20]. SNA has been shown to have strong influence over arterial vasomotion, as suggested by data from patients with autonomic dysfunction who exhibit loss of vasomotion in peripheral vasculature[21]. These results, and others not described, support the notion that sympathetic nervous outflow is critical in the appearance of vasomotion *in situ*.

1.3) Biosensor Theory

ExMLCK, a FRET-based Ca^{2+}/Calmodulin sensor molecule, has permitted measurement of [Ca^{2+}] in arterial vasculature in several experimental preparations[22]. In addition, the biosensor allows for correlation between molecular dynamics and mechanical activity of VSM. VSM activation is preceded by Ca^{2+} entry into the cell (as well as from internal stores), which serves to activate the contractile mechanism. More specifically, Ca^{2+} binds to Calmodulin, which then binds to exMLCK. This binding 1) decreases FRET between CFP and YFP by inducing a conformational change in exMLCK and 2) activates potential myosin light chain kinase activity[22]. Because of this mechanism, the amount of FRET between the two fluorescent moieties is directly proportional to the fraction of exMLCK molecules bound to Ca^{2+}/Calmodulin.

To quantify this, fluorescence ratios (R) are used, defined as the CFP fluorescence emission divided by the YFP fluorescence emission. In exMLCK, maximum FRET occurs when no Ca^{2+}/Calmodulin is bound. In this case, CFP (donor) fluorescence is minimal and YFP (acceptor) fluorescence is maximal. Thus, there is a minimum ratio, R_{min}, when [Ca^{2+}] is zero. A maximum ratio, R_{max}, occurs when all exMLCK is bound to Ca^{2+}/Calmodulin. R_{min} and R_{max} represent 0% and 100% fractional occupancy of exMLCK by Ca^{2+}/Calmodulin.

The fractional occupancy of exMLCK by Ca^{2+}/Calmodulin (symbolized here as Y) can then be calculated as:

$$Y = \frac{R - R_{min}}{R_{max} - R_{min}} \qquad \textbf{Eqn. 1}$$

Free intracellular [Ca^{2+}] is then derived from Y, using the Hill equation, as

$$\left[Ca^{2+}\right] = \left(\frac{Y * {K_{D,app}}^{n}}{1 - Y}\right)^{1/n} \qquad \textbf{Eqn. 2}$$

where $K_{D,app}$ is the apparent dissociation constant derived from the law of mass action and n is the Hill coefficient. Previous work has shown that the relationship between free [Ca^{2+}] and exMLCK FRET ratio, R, as measured in α-toxin permeabilized mesenteric small arteries, is well fitted by the Hill equation, with a EC_{50} ($K_{D,app}$) of 0.891 μM (pCa, 6.05) and a Hill coefficient (n) of 1.4 (see figure I) [5].

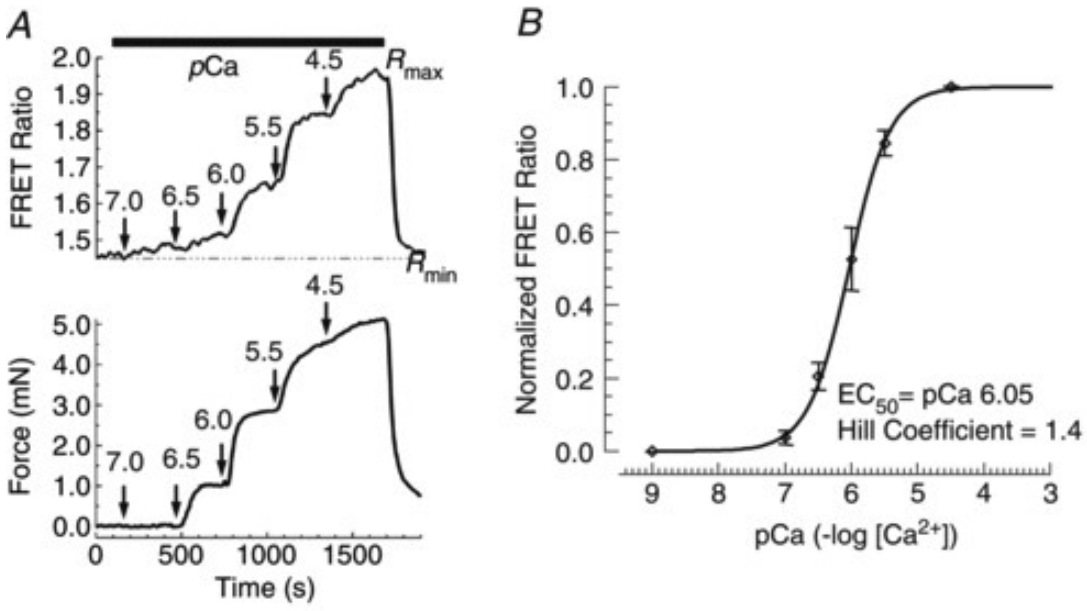

Figure I – Calibration of [Ca^{2+}] to exMLCK FRET ratio via α-toxin permeabilized arteries.

Panel A – An isolated, permeabilized murine mesenteric artery mounted on a confocal wire myograph subjected to various [Ca^{2+}] solutions. Upper plot shows relationship between FRET ratio and pCa, while the lower plot shows force changes with varying [Ca^{2+}] solutions.

Panel B – pCa-FRET ratio relationship. The curve was generated using the same data from FRET ratios obtained in *A*. Normalized FRET ratio is calculated using eqn. 1 (above). (Adapted from Wang *et al*[5]. Used with permission from Wang *et al*, Journal of Physiology.)

This method is valid if all fluorescence emission detected arises only from FRET interactions between the two fluorophores. Intrinsic fluorescence of smooth muscle via NAD(P)H and flavins confounds the fluorescence emission data and can lead to inaccurate quantification of intracellular Ca^{2+}. Described in more detail in the following chapters, the use of two-photon microscopy obviates these issues, allowing for robust measurements of Ca^{2+} signaling events *in vivo*.

In addition to exMLCK, an additional protein-based fluorophore was used in the study. GCaMP2, a derivative of its predecessor GCaMP, is a GFP- and intensity-based protein that has been implemented in numerous studies of Ca^{2+} signaling in various tissues[3]. The protein provides non-ratiometric measure of $[Ca^{2+}]$ in VSM with high spatiotemporal resolution.

1.4) Goals

Here we utilized genetically encoded calcium indicators (GECI) specifically expressed in arterial VSM, along with Förster resonance energy transfer (FRET)-based two-photon microscopy, to design a method for measuring Ca^{2+} signaling in a fully conscious, head-fixed mouse. The ratiometric design of the FRET-based GECI allows for quantification of VSM $[Ca^{2+}]$ in the unadulterated physiological environment, a task previously impossible due to limitations in experimental design. Specifically, we sought to: 1) quantify VSM $[Ca^{2+}]$ in peripheral vascular beds of conscious head-fixed mice and those subjected to isoflurane anesthesia and sympatholytic treatment, 2) assess the effect of isoflurane anesthesia and sympathetic nervous system blockade on prevalence and frequency of vasomotion, and 3) evaluate the effect of hypertension on prevalence of vasomotion. It is our hypothesis that SNA is the driving factor for appearance of vasomotion *in vivo* and that acute blockade or augmentation of SNA will result in the modulation of vasomotion.

This thesis is organized in the following manner: Chapter 2 will describe the methods and materials used to achieve the aforementioned goals. Chapter 3 will present the results from application of said methods, and chapter 4 will summarize the results and interpret their meaning. Supplemental graphics can be found online at drum.lib.umd.edu.

Chapter 2: Methods and Materials

2.1) Animals

Two types of mice that express genetically encoded fluorescent biosensors molecules specifically in smooth muscle cells were used. Here, these are referred to as "exMLCK" and "GCaMP2". ExMLCK contains a short form myosin light chain kinase (MLCK) fused to enhanced cyan fluorescent protein (ECFP) and yellow fluorescent protein (YFP) linked by the rabbit smooth muscle MLCK-Calmodulin binding sequence[22]. In exMLCK mice, the transgene is under control of the smooth muscle α-actin promoter and the genetic background is the Inbred Charles River (ICR) strain. Incorporation of exMLCK was shown to not effect animal weight, heart rate, arterial blood pressure, and smooth muscle force development despite being expressed at about 30% the level of endogenous MLCK[22].

GCaMP2 mice contain the transgene for an enhanced form of the circularly permuted chromophoremodulating Ca^{2+}biosensor molecule, GCaMP. GCaMP2 contains several mutations that elicit improved brightness, thermal stability, and dynamic range as compared to GCaMP. These properties have allowed for the measurement of Ca^{2+} signaling in hearts[23] and vascular endothelium[24]of mice *in vivo*. The GCaMP2 transgene was placed under transcriptional control of a ~16 kb smooth muscle myosin heavy chain promoter[25]. The gene construct was injected into oocytes and the lines with high expression were selected and maintained on a C57B1/6 background. GCaMP2 mice were used solely to assess the prevalence of vasomotion, as the non-

ratiometric design of the indicator precludes quantification of Ca^{2+} signaling without making assumptions about the [Ca^{2+}] corresponding to baseline fluorescence.

All mice were maintained on a 12:12-h light/dark schedule at 22-25° C and 45-65% humidity and fed *ad libitum* on a standard rodent diet and tap water. Only mice aged 12-20 weeks were used. All procedures and experiments were approved by the Institutional Animal Care and Use Committee of the University of Maryland School of Medicine.

2.2) Radio Telemetric Recording of Blood Pressure

Arterial blood pressure monitoring was achieved via procedures described previously[2, 3]. In short, 2% isoflurane supplemented with 100% O_2 was used to maintain anesthesia during the implantation procedure. Following cleaning with povidone-iodine solution (Betadine, Purdue Products L.P, Stamford, CT, USA), a 1 cm mid-sagittal anterior neck incision was performed. Subsequently, the right common carotid artery was exposed and ligated. The catheter tip containing the pressure transducer (DSI TA11PA-C10, Data Science International, Minneapolis, MN, USA) was inserted proximal to the ligature and was passed to the origin of the carotid at the aortic arch. Suture was subsequently applied prevent catheter migration during locomotion and the dissection was sealed with adhesive (Vetbond, 3M, St. Paul, MN, USA). The body of the sensor was passed through a subcutaneous pocket created from blunt dissection of anterior abdominal wall. Animals were allowed to recover for 7-10 days before use in the study. DSI telemetric receivers and software

were used to record the blood pressure data. Blood pressure data was sampled at 500 Hz.

2.3) Installation of Head Restraints

Mice were sedated using the same anesthesia protocol as described above. The mouse scalp was subsequently trimmed using hair clippers and cleaned with a povidone-iodine solution. The dorsal skin surface was removed via surgical scissors. The underlying periosteum was removed via scraping with sterile cotton swab, which was also implemented to dry the skull surface. With the aid of a dissection microscope, two tap holes were drilled on, but not through, the parietal bone approximately 3-5 mm caudal and 2 mm lateral to bregma. The tap holes were filled with two miniature screws about 0.4 mm in diameter (J.I. Morris Company, Southbridge, MA, USA), which served to provide increased adhesion between the skull and the bonding agent. A 2.5 cm threaded stainless steel bar was secured in a horizontal position closely opposed to the skull, extending away from the experimental ear, via dental cement (Dentsply, York, PA, USA). The animals were allowed to recover for 3 days before use in the study. During the imaging procedure (described below), animals were anchored to the stage atop a custom treadmill with variable resistance to locomotion.

2.4) Imaging of Mouse Ear

Arterioles of the ear were chosen for imaging, as they are accessible optically with two-photon microscopy. As the peripheral vasculature of the ear is highly innervated

by the sympathetic nervous system, the site was appropriate for our investigations here. Hair on the dorsal ear was carefully depilated (Nair; Church & Dwight Co., Inc., Princeton, NJ) at least 3 days prior to imaging. Mice were anesthetized using isoflurane (2%, 1.6% for induction, maintenance respectively) and mounted on the treadmill system described above. The ventral surface of the ear was affixed to a silicone platform using adhesive tape, allowing for access to the dorsal ear for imaging. A polypropylene ring was used to contain the water used with the dipping objective lens (20x, 1.0 NA). The objective lens was heated with a feedback-controlled temperature controller set to 37.0° C to maintain ear temperature while imaging.

While imaging in the conscious state, mice were taken off isoflurane and allowed to regain consciousness inside the darkened platform of the upright microscope. Mice were allowed to acclimate to the imaging platform for at least 10 minutes before imaging began. Thermal equilibrium between the temperature-controlled objective and the mouse ear was established in this time. Increased resistance to locomotion was achieved by increasing friction at the rotation axis and discouraged excessive activity while on the imaging platform. The figure below depicts the aforementioned components and orientation of the animal during imaging (see figure II). An example video of image acquisition is included in the supplemental files (see supplemental video #1).

Figure II – *In vivo* imaging setup.

Panel A – Picture of imaging platform demonstrating: 1) Objective lens (described in detail below) opposed to the pinned mouse ear, 2) the custom built poly(lactic acid) treadmill with adjustable resistance to locomotion, 3) video camera with IR filter to visualize conscious mouse while mounted on the imaging platform.

Panel B – Picture of the mouse ear pinned to the silicone platform. The ear is affixed to the platform using adhesive tape, allowing the dorsal ear to be imaged. Water for the dipping objective lens was retained using the polypropylene ring. The blood pressure transducer can be seen on the left abdomen of the animal.

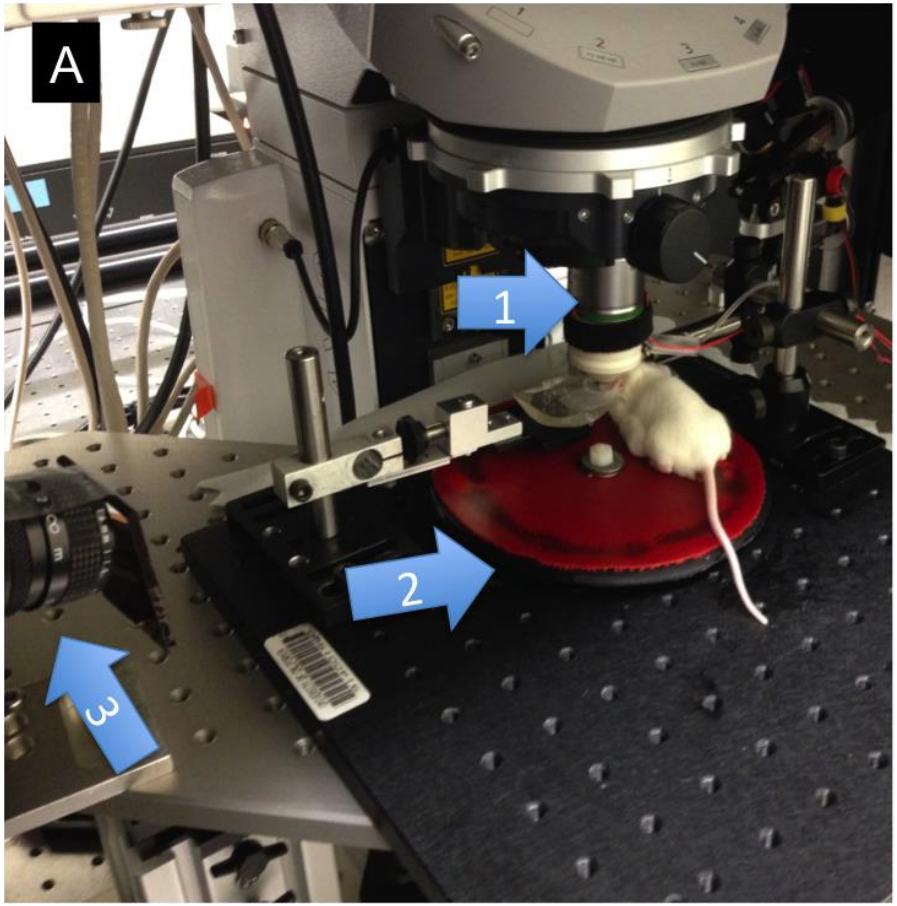
A
1
2
3

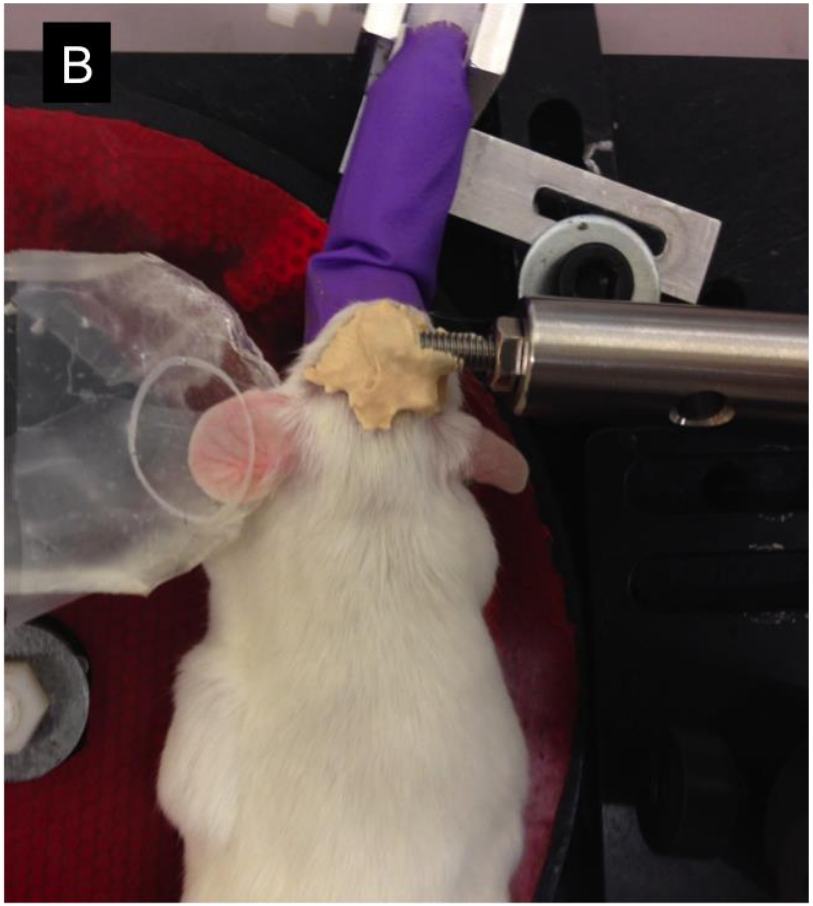
B

Arterioles were selected for imaging on the basis of superficiality of the ear vessels of interest and strength of expression using epifluorescence excitation and emission filtering for direct visualization of the YFP moiety of exMLCK (same for GCaMP2 mice, but GFP was visualized).

2.5) Fluorescence Recording

To quantify intracellular calcium and vessel diameter we used a Zeiss 7MP microscope with a femtosecond pulsed near infra-red (IR) laser (Cameleon Vision, Coherent, Inc., Santa Clara, CA) for two-photon microscopy. A Zeiss 20x water plan-apochromat with a working distance of 1.9 mm and a NA of 1.0 was utilized. Scanning was bi-directional at frame rates of 1.36 Hz and pixel sizes of 0.40-0.63 μm, depending on site of image acquisition. The microscope was situated inside a light-tight enclosure and imaging was performed with room lights off to minimize background noise.

exMLCK: ExMLCK FRET measurements were performed by selective excitation of the CFP moiety at 820 nm. Previous work has shown that YFP excitation at this wavelength is minimal[3]. CFP and YFP emission was band pass filtered from 460 to 500 nm and 520 to 560 nm, respectively. Two binary GaAsP photodetectors within the Zeiss 7 MP detected fluorescence emission. The gains of the two detectors were held constant throughout all experiments at levels optimizing exMLCK fluorescence signal. These gains were used during calibration experiments, which elucidated the

maximum and minimum FRET ratios obtainable from our microscope. Polystyrene beads labeled with recombinant CFP and YFP revealed that direct excitation of YFP at 820nm was negligible (data not shown) and that 17% of the fluorescence signal in the CFP channel, F_{CFP}, appeared in the YFP channel, F_{YFP}, as a result of 'spectral overlap' (see figure III). exMLCK fluorescence ratios (R) were therefore calculated as:

$$\boldsymbol{R = \frac{F_{CFP}}{F_{YFP} - 0.17 * F_{CFP}}} \qquad \textbf{Eqn. 3}$$

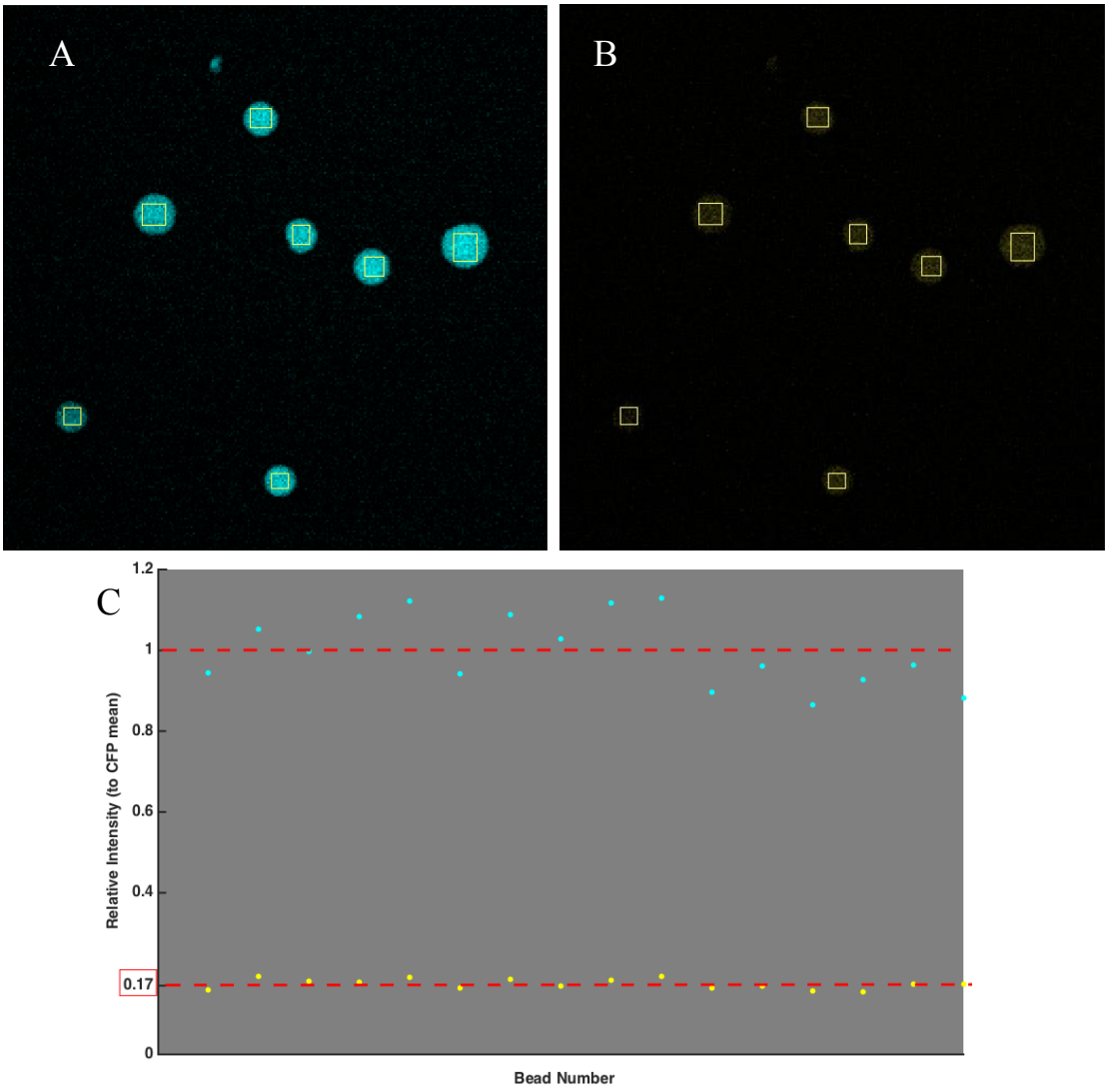

Figure III – Determination of CFP signal detected in YFP channel at exMLCK excitation wavelength.

Panel A,B – Example of ROIs within polystyrene beads labeled with ECFP used in determination of correction factor in eqn. 3. *A* and *B* show the signal obtained in the CFP and YFP channel, respectively.

Panel C – The correction factor was calculated by quantifying the relative CFP signal obtained in the YFP channel. The mean value of the YFP signal was normalized to the mean CFP signal obtained at the relative detector gains.

GCaMP2: Excitation at 920 nm was found to produce optimal signal. Tissue intrinsic fluorescence, as measured in GCaMP2 -/- mice, was absent when excited at 920 nm.

2.6) exMLCK Calibration Experiments

Maximum and minimum fluorescence ratios, R_{max} and R_{min} respectively, are not constants but depend on the optical setup (photodetector gains, optical elements, etc). As direct exposure to external 0 [Ca^{2+}] and high-[K^{+}] solutions (providing R_{min} and R_{max}, respectively) *in situ* is impossible in the intact ear vasculature, small mesenteric arteries were imaged with exactly the same experimental conditions and acquisition settings used for the *in vivo* experiments (except for experiments using hypertensive mice, which were examined using different conditions which were not calibrated for ratiometric measurement). Isolated mesenteric arteries, subjected to both external 0 [Ca^{2+}] solution and subsequent depolarization in 117 mM K^{+} solution, provided a minimum and maximum [Ca^{2+}] state. R_{min} and R_{max} were estimated for experiments using hypertensive mice.

To examine the isolated mesenteric arteries, mice were anesthetized under isoflurane (2%) and euthanized via cervical dislocation. The mesenteric arcade was exteriorized via midline incision and retraction of the intestines. After excision, the arcade was immersed and held in a “dissection solution” composed of (in mM): MOPS, 2; NaCl, 145; KCl, 4.7; $CaCl_2$, 2; $MgSO_4$, 1.2; $NaH2PO_4$, 1.2; EDTA, 0.02; pyruvate, 2; glucose, 5; 1.0% albumin (pH 7.4). 2mm segments of third and fourth order vessels,

ranging from 100-200 μm in diameter, were mounted isometrically by being pulled over a glass cannula. The proximal end of the vessel was cannulated first, then gently ligated using 10-0 Ethilon ophthalmic nylon suture (Ethicon, Somerville, NJ). Gentle flushing of the vessel through the cannula was performed to remove blood from the lumen. Subsequently, the distal end was cannulated and secured via suture and the vessel was pressurized to physiologic pressure (70 mmHg). One cannula was attached to a servo-controlled pressure-regulating device (Living Systems, Burlington, VT), whereas the other was attached to a closed stopcock. Arterial segments were continuously superfused with warmed solution containing (in mM) NaCl, 112.0; $NaHCO_3$, 25.7; KCl, 4.9; $CaCl_2$, $MgSO_4$, 1.2; KH2PO_4; 1.2, glucose, 11.5; and HEPES,10.0 (pH 7.4, gas composition: 5% O_2-5% CO_2-90% N_2) at 37°C and were studied in the absence of intraluminal flow. High (117 mM) external K^+ solution was made by replacing NaCl with equimolar KCl of normal PSS. Ca^{2+}-free solution was made by omitting Ca^{2+} and adding 2.0 mM EGTA (pH 7.4). The solutions were superfused into the recording chamber at a constant flowrate of 1.5 mL/minute.

Intrinsic fluorescence arising from the basal lamina and adventitia could possibly confound the measurement of exMLCK FRET emission. To avoid this, the vessel was imaged through the luminal center (VSM cells in cross-section). The high spatial resolution of two-photon microscopy (granted by a small excitation volume) is advantageous here; it can be assured that this intrinsic fluorescence is not present when excitation occurs within the VSM cell. In addition, NAD(P)H is not excited at

wavelengths greater than 800 nm[26], yielding low intrinsic fluorescence of the VSM cytoplasm itself.

2.7) Experimental Hypertension

Experimental hypertension was elicited via subcutaneous implantation of an Alzet osmotic mini-pump (Model 1003, Durect, Cupertino, CA) loaded with Angiotensin-II (ANG-II). ANG-II was delivered at a constant flow rate of 350 $ng*kg^{-1}*min^{-1}$ for 5 days. Animals were also fed a high-salt diet [6% NaCl (wt/wt)] during the infusion period. Previous studies utilizing the same procedure have shown a 26 mmHg increase in MAP when subjected to ANG-II/salt[3].

2.8) Intraperitoneal (i.p.) Injections

Brief "twilight" anesthesia, unassociated with hemodynamic changes as measured by telemetry, was administered to blunt locomotor response to injection. This approach was taken to ensure the animal was not experiencing pain or discomfort whilst mounted on the imaging platform. The injection was performed via 26.5 gauge needle angled 30° relative to the spinal cord axis in the lower right quadrant of the abdomen[27]. Hexamethonium 30 μg/g BW (Sigma-Aldrich, St. Louis, MO) dissolved in sterile saline (0.9% NaCl) was delivered to achieve ganglionic blockade. Imaging in the ganglionic blockade state was performed during a 20-minute period beginning 10 minutes post-injection (see figure IV).

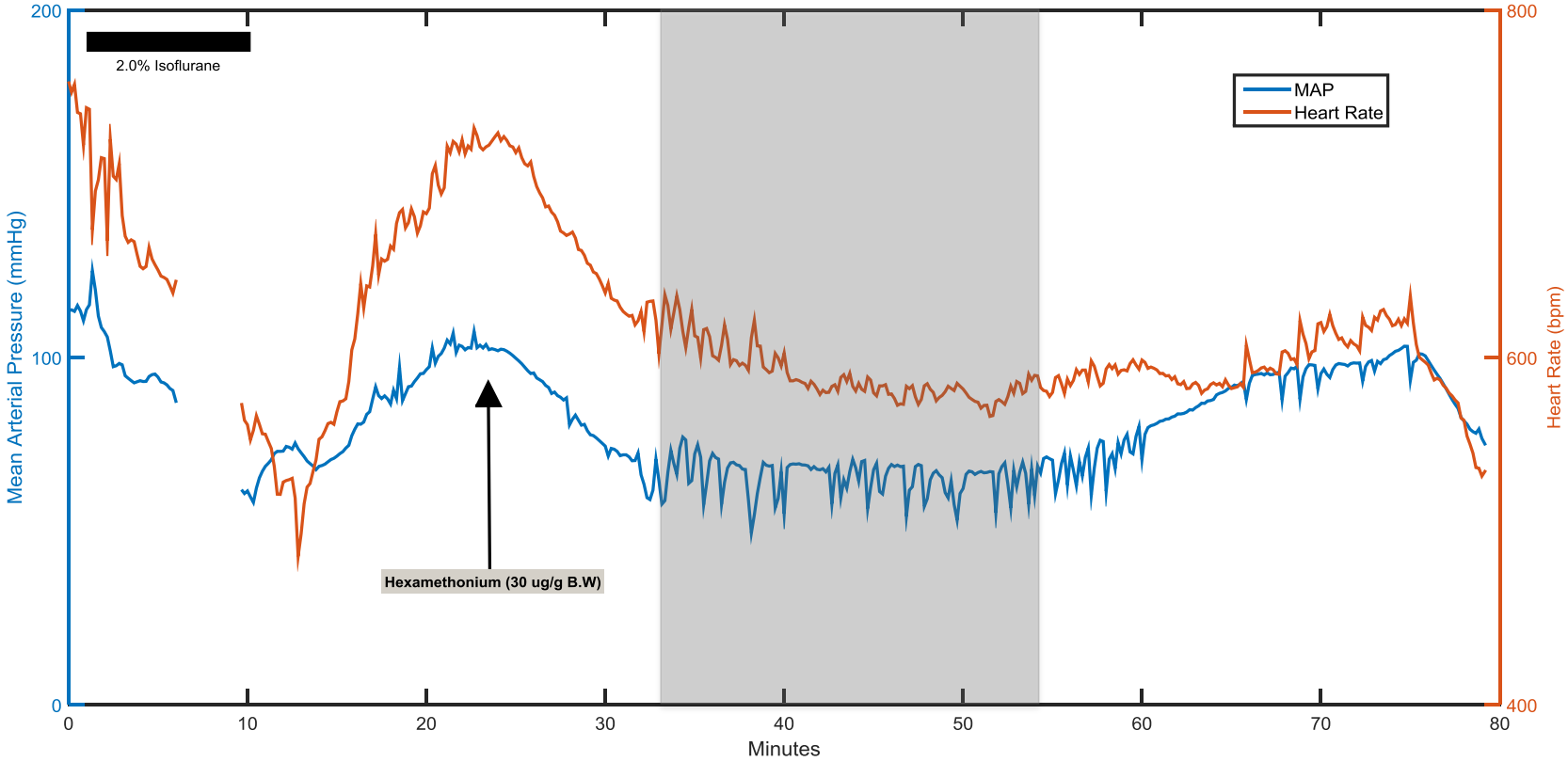

Figure IV – Hemodynamic response to ganglionic blockade via i.p hexamethonium.

A graph of the hemodynamic responses to experimental protocol. Upon 15 minute recovery from anesthesia, hexamethonium was delivered i.p following the procedure described above. The gray area delineates the 20 minute window for imaging post-injection.

2.9) Data Analysis and Statistics

Data are expressed as means +/- s.e.m.; *n* denotes the number of animals. Comparisons of ordinal data were made using Student's paired or unpaired t-test, as appropriate. Nominal data, like the presence of vasomotion, was analyzed with the exact binomial test. Differences were considered significant at $P < 0.05$. MATLAB (Mathworks, Natick, MA) and Microsoft Excel® (Microsoft, Redmond, WA) was used for generating graphics. Blood pressure measurements were analyzed using DSI software. Vasomotion was deemed to be present if ≥ 2 contraction-dilation cycles were noted during image acquisition (with appropriate Ca^{2+} signaling).

Image processing and non-parametric power spectral analysis was via custom software routines using IDL (Exelisvis, CO). Direct spectral analysis of the blood pressure data was made possible by a constant sampling rate of 500 Hz.

Chapter 3: Results

3.1) Calibration Experiments

Two (n=1) small mesenteric vessels were imaged under the conditions described in the methods section. A robust response to depolarizing solution was seen, as the vessels constricted from 230.43 ± 6.7 μm to 88.0 ± 3.5 μm. Because expression of exMLCK is not constant throughout the VSM cells, the image data was masked to exclude dim regions of interest (ROIs) within the vessel, as seen in the figure below (figure V). After analyzing 5 ROIs from each experiment, R_{min} was determined to be 2.1 ± 0.07 and R_{max} was determined to be 4.25 ± 0.07.

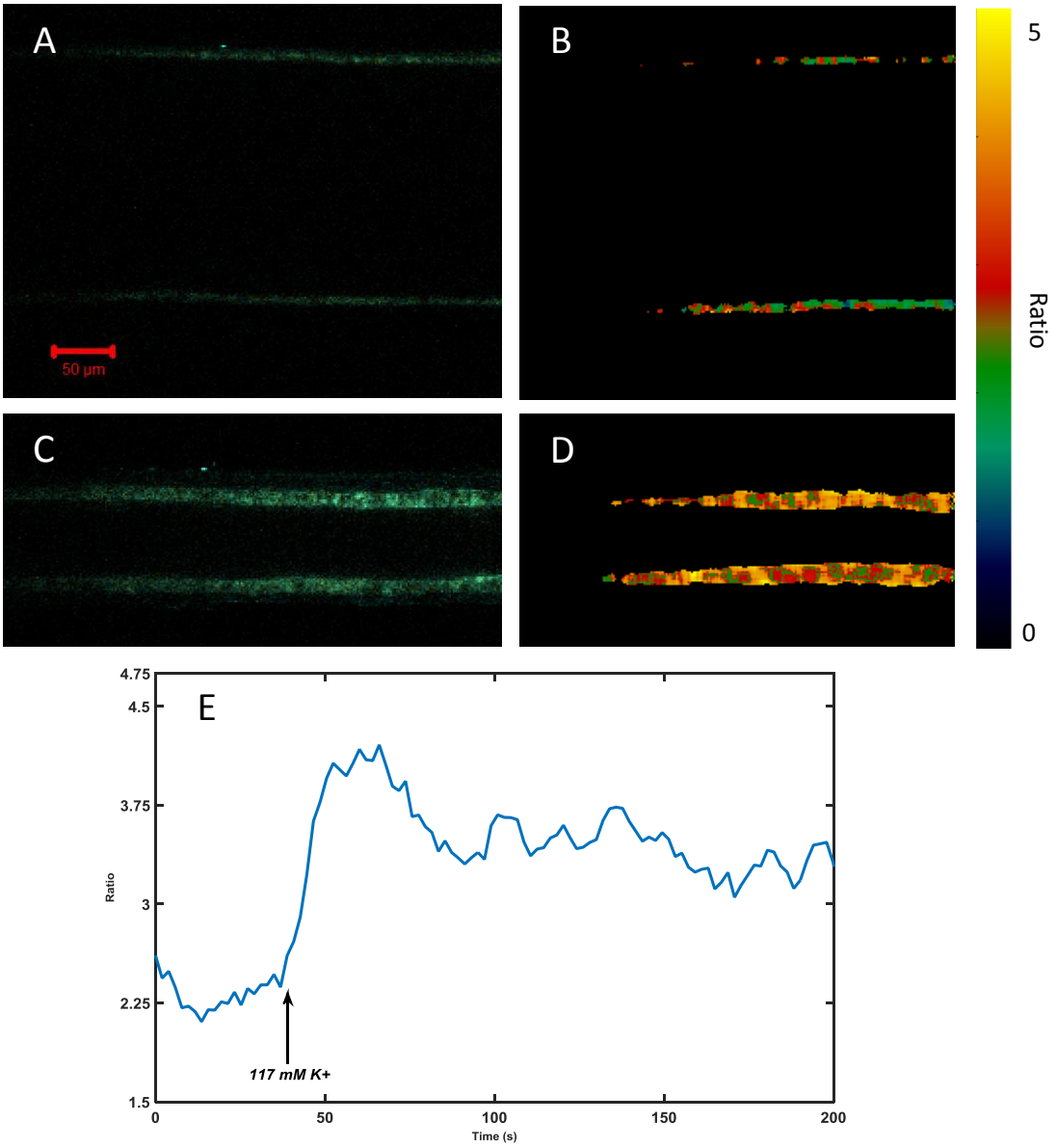

Figure V – exMLCK calibration experiment.

Panels A,C – Representative example of raw composite images (CFP and YFP) of the isolated mesenteric arteries used in the calibration experiment. The scale bar applies to panels *A*-*D*.

Panels B, D – Masked images of the arteries shown in *A* and *C*. Rainbow-colored images depict the range of calculated FRET ratios from Ca^{2+}-free solution (*panel B*) and 117 mM K^{+} solution (*panel D*).

Panel E – Graph shows ratio as a function of time in a region of interest (ROI) before, during, and after switch from the R_{min} solution (0 $[Ca^{2+}]$) to the R_{max} solution (117 mM K^{+}). In this representative ROI, R changed from ~2.2 to 4.2.

3.2) Hemodynamics

Hemodynamic measurements began as the animal was in the housing cage before anesthesia and continued into induction with 2% isoflurane. To evaluate the effects of restraint and darkness on hemodynamics, we compared the MAP of the conscious unrestrained animal to that of the head-fixed animal (n = 2). Interestingly, MAP was very similar between the two states (103.0 ± 5.0 mmHg and 104.3 ± 4.7 mmHg, conscious unrestrained and head-fixed, respectively) as well as heart rate. Anesthesia reliably depressed MAP and heart rate (76.0 ± 3.5 mmHg and 561.3 ± 9.1 bpm, respectively, $P < 0.05$). Because two-photon microscopy was employed, the immediate environment of the animal upon recovery from anesthesia was that of darkness. As expected, hexamethonium significantly lowered MAP and HR (71.9 ± 4.7 mmHg and 589.6 ± 4.4 bpm, $P < 0.05$). Occurrences of attempted locomotion decreased under hexamethonium (data not shown) and were accompanied by paradoxical reductions in MAP (see figure IV). The hemodynamic responses to experimental intervention are summarized in the figure below (figure VI).

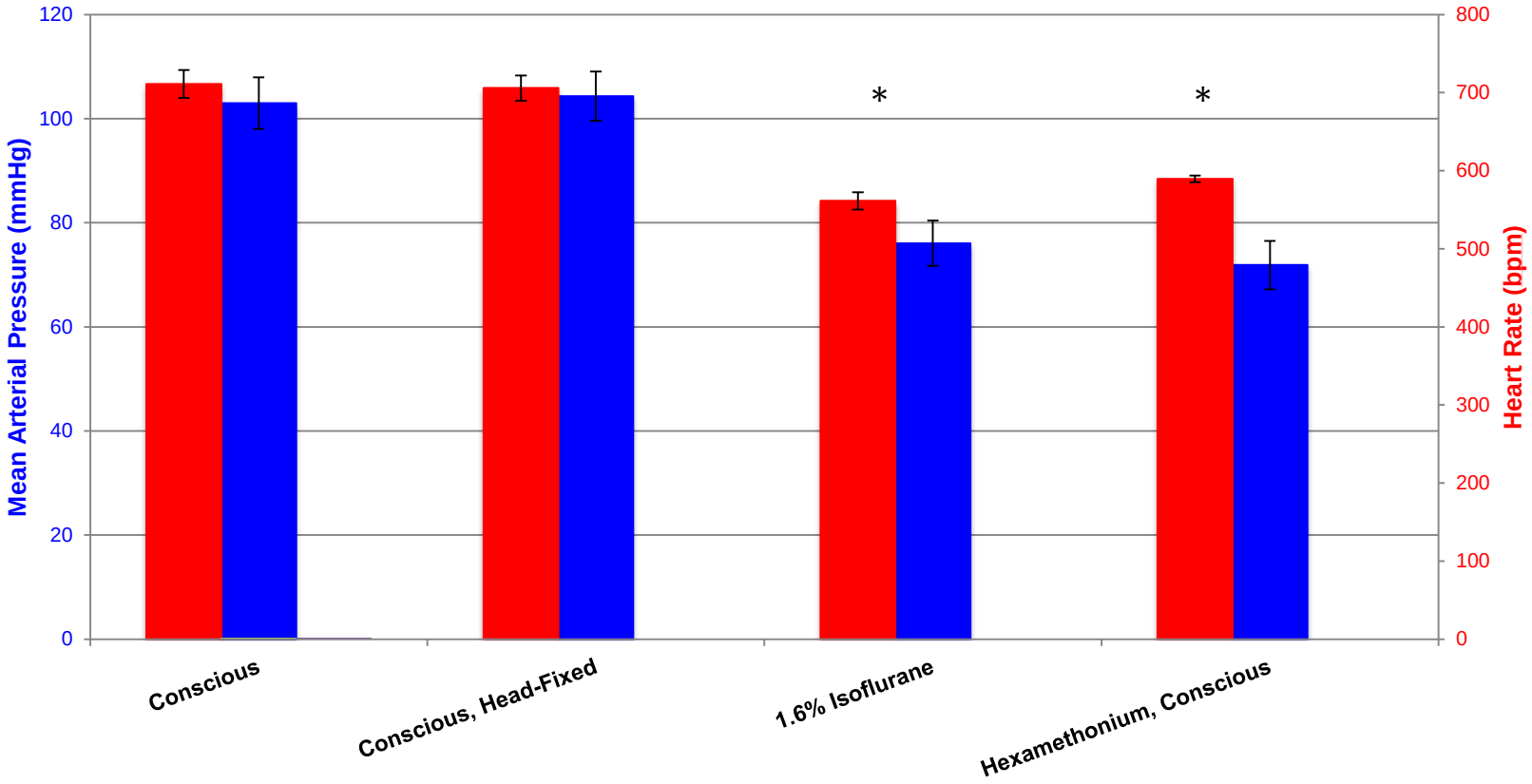

Figure VI – Hemodynamic responses to experimental intervention.

Summary data (n =2) demonstrate that heart rate (shown in red) and MAP (shown in blue) are unaltered during the conscious head-fixed state. Both i.p hexamethonium and 1.6% isoflurane decreased MAP and heart rate significantly as compared to the conscious state (* $P < 0.05$).

Power spectrum analyses of arterial blood pressure are commonly used to assess autonomic nervous system control of the cardiovascular system in humans and other species[28-30]. In mammals, a low frequency (LF) component (0.6-1.5 Hz in mice, also termed Meyer waves) of the power spectrum is attributed to sympathetic control of blood pressure as sympathomodulatory pharmacological treatment elicits appropriate increases or decreases in power in this bandwidth. A higher frequency (HF) component (2.5-5.0 Hz in mice) has been associated with vagal/parasympathetic control, synchronous with respiration (respiratory sinus arrhythmia). Changes in the ratio of LF:HF power, found by integrating the power spectral density (PSD) curve in the aforementioned bandwidths, is a reliable index of sympatho-vagal interaction[30-32]. A representative example of power spectral change in response to isoflurane anesthesia and hexamethonium is shown in the figure below (figure VII). Administration of both isoflurane and hexamethonium reduced power in the region as expected. LF:HF power ratio in this animal decreased from 12.5 in the conscious state to 1.6 and 0.16 in the ganglionic blockade and anesthetized states, respectively.

Figure VII – Power spectral density of MAP variability in experimental conditions.

Panel A - Representative example of power spectrum elicited by non-parametric methods (i.e, fast fourier transform). The low-frequency component (0.15 – 0.6 Hz), depicted by the magenta bar, of the curve is attenuated dramatically with isoflurane anesthesia and ganglionic blockade. This bandwidth reflects sympathetic control in the adult mouse. The cyan bar, spanning 2.5 – 5.0 Hz, represents the high-frequency component of blood pressure variability and is attributed to parasympathetic/vagally-mediated control.

Panel B - LF:HF ratio in the 3 experimental conditions. In this example, the ratio decreased from 12.5 in the conscious state to 1.6 and 0.6 in ganglionic blockade and 1.6% isoflurane, respectively.

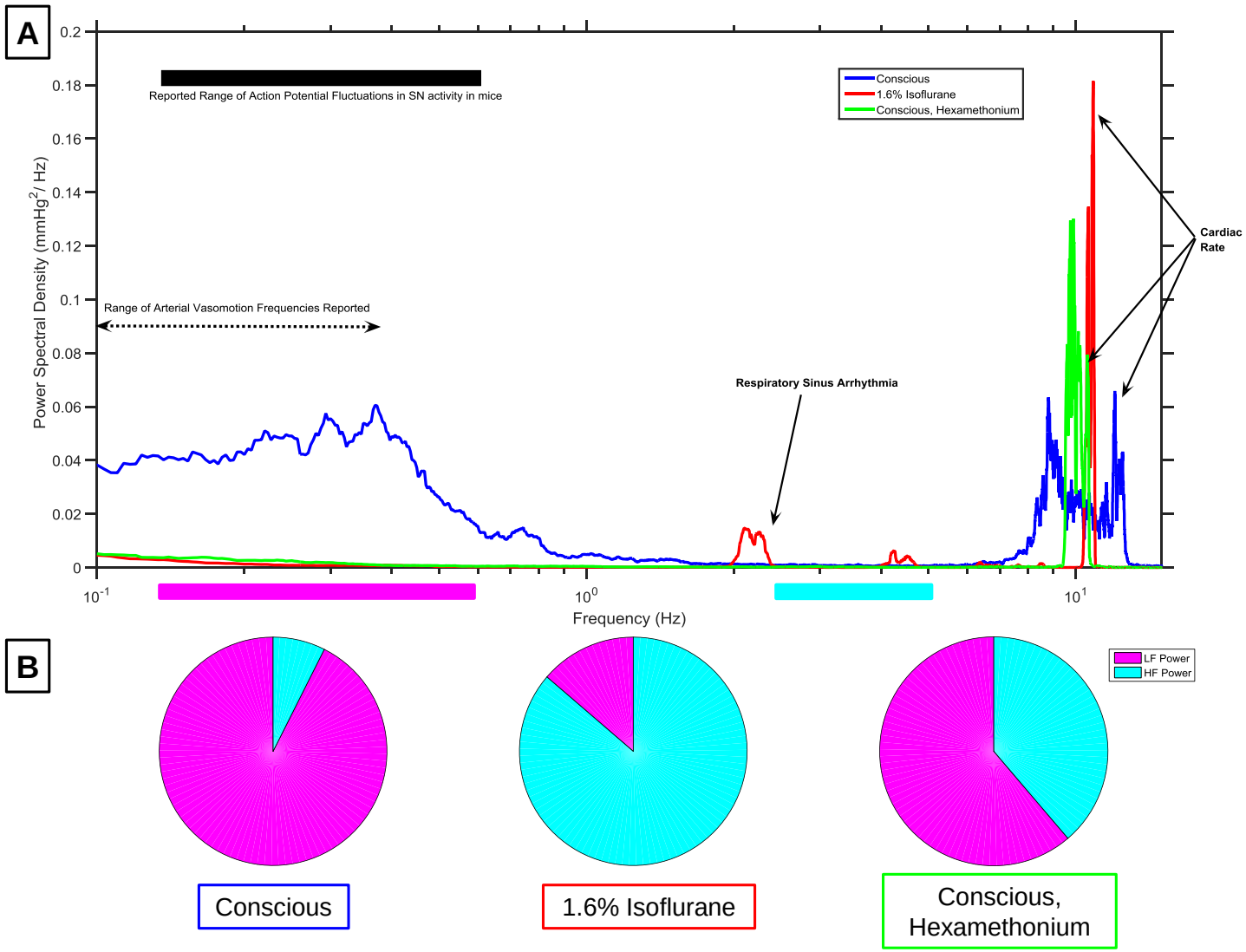
A
Reported Range of Action Potential Fluctuations in SN activity in mice
Conscious
1.6% Isoflurane
Conscious, Hexamethonium
Cardiac Rate
Range of Arterial Vasomotion Frequencies Reported
Respiratory Sinus Arrhythmia
Power Spectral Density (mmHg^2/ Hz)
Frequency (Hz)
B
LF Power
HF Power
Conscious
1.6% Isoflurane
Conscious, Hexamethonium

ANG-II/salt, delivered with the same protocol as described here, produced pronounced hypertension in previous studies with exMLCK and GCaMP2 mice, increasing MAP up to 26 mmHg in the first 4 days of treatment[3]. Power spectral analysis was employed to characterize SNA during experimental hypertension. Shown in the figure below, (figure VIII), LF power and LF:HF ratio decreased progressively from baseline to day 4 of ANG-II/salt. LF:HF power ratio at baseline was calculated as 8.4 ± 2.4 and decreased to 0.4 ± .3 and 0.8 ± 0.4 on days 3 and 4 respectively (P = 0.03 and = 0.049 for days 3 and 4, respectively; n = 3).

Figure VIII – Power spectral density changes in ANG-II/salt hypertension.

Panel A – Representative blood pressure power spectra in ANG-II/salt from one animal. The blue, red, and green curves correspond to baseline, day 3 and day 4 post-pump implant, respectively. As shown in figure VII, the magenta and cyan bars represent the LF and HF bandwidths used for calculation of the LF:HF power ratio. The LF component is attenuated progressively in the first 4 days of ANG-II salt. The heart rate of this animal decreased from baseline during ANG-II/salt intervention.

Panel B – LF:HF power ratio during ANG-II salt. On average (n = 3), LF:HF power ratio decreased from 8.4 to 0.4 and 0.8 on days 3 and 4 of experimental hypertension.

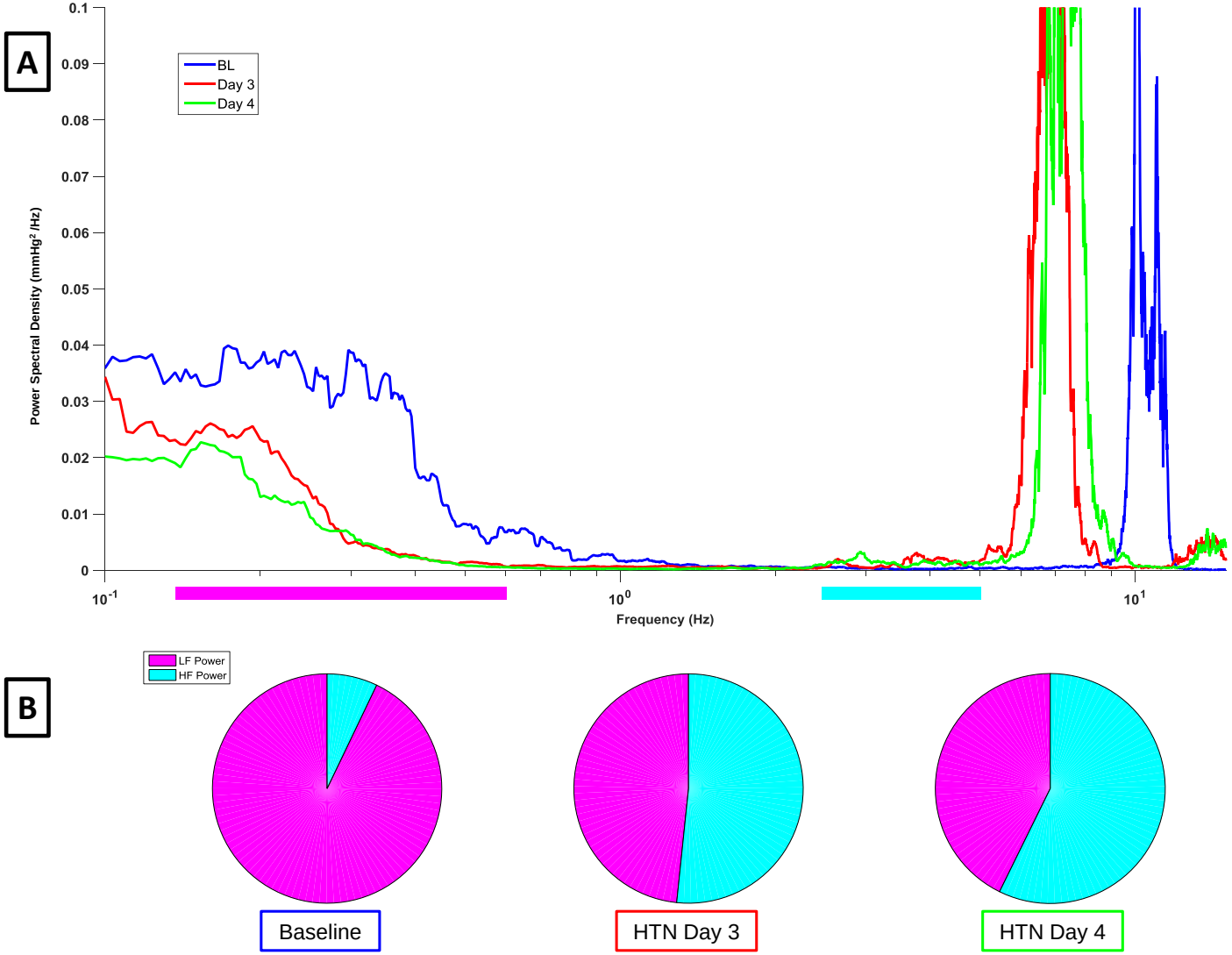
A
BL
Day 3
Day 4
Power Spectral Density (mmHg² /Hz)
0.1
0.09
0.08
0.07
0.06
0.05
0.04
0.03
0.02
0.01
0
10^-1
10^0
10^1
Frequency (Hz)
B
LF Power
HF Power
Baseline
HTN Day 3
HTN Day 4

3.3) Vasomotion

11 paired arterioles, ranging in time-averaged diameter of 28.0 μm to 67.3 μm, were imaged in the conscious restrained state and under maintenance of isoflurane anesthesia (n=4, all exMLCK). Administration of isoflurane did not result in a significant change in time-averaged arteriolar diameter ($P = 0.10$), but did reduce prevalence of vasomotion as compared to the conscious, head-fixed state (82% to 36%, $P = 0.03$). Upon stratification by vessel diameter in the conscious head-fixed state, no clear pattern of change (either vasodilation or vasoconstriction) was found upon administration of isoflurane (figure IX).

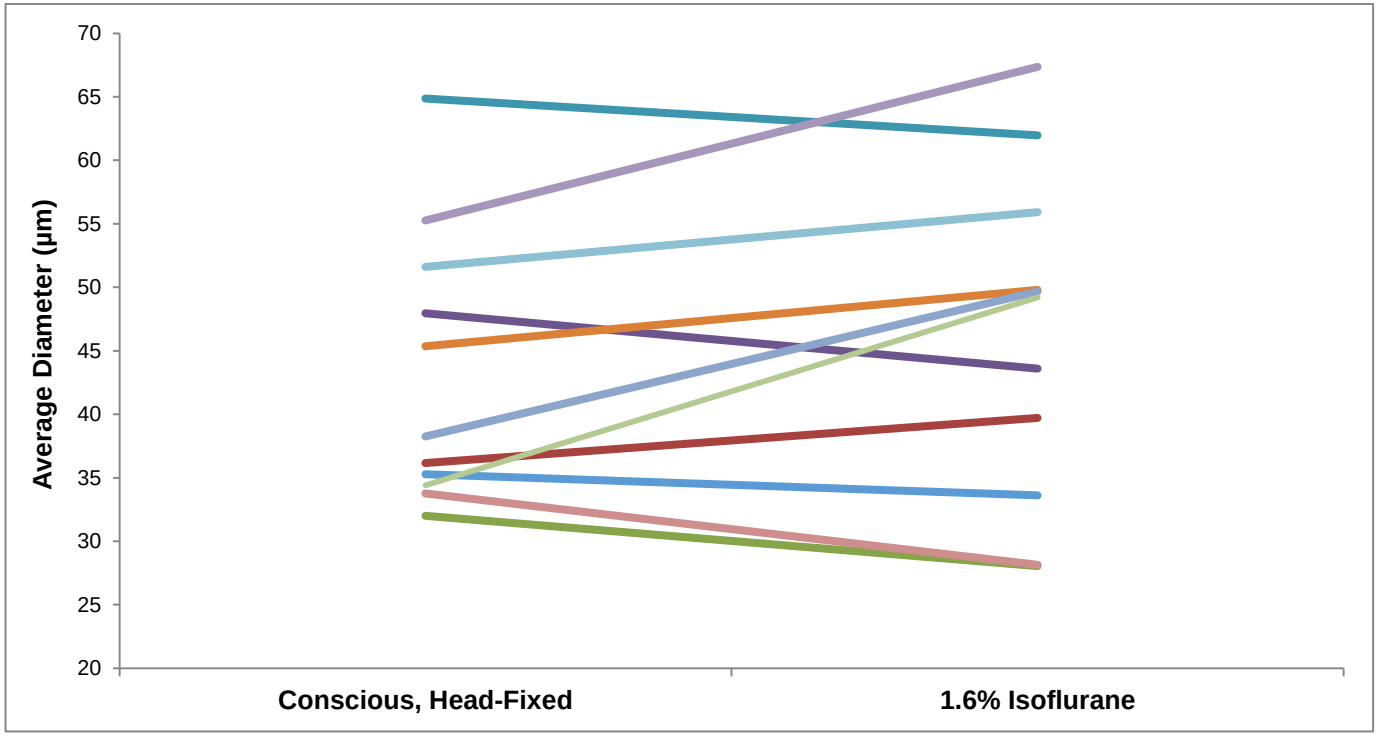

Figure IX – Peripheral arteriolar tone responses to 1.6% isoflurane.

Time-averaged diameter of 11 paired arterioles in the conscious, head-fixed state and under 1.6% isoflurane anesthesia. Variable responses were seen, as some vessels changed minimally while others exhibited marked vasoconstriction or vasodilation. Upon stratification by diameter in the conscious, head-fixed state, no discernable pattern of tone response could be elucidated.

Three arterioles (n=1) were found to be undergoing vasomotion in both the conscious head-fixed and anesthetic state. We sought to characterize the frequencies of oscillation via power spectral density analysis of diameter changes in both states. High-pass filtering at 0.02 Hz was applied to eliminate high frequency signals resulting from stochastic background noise detected during image acquisition. In the conscious, head-fixed state oscillatory vasomotion occurred at a frequency of ~0.25 Hz, while the same vessel under isoflurane anesthesia exhibited more rapid vasomotion at a frequency of ~0.35 Hz (figure X). Interestingly, the power spectrum of diameter changes associated with vasomotion in the isoflurane state revealed two predominant frequencies while arterioles in the conscious, head-fixed state oscillated in one frequency.

Figure X – Characterization of vasomotion exhibited under isoflurane anesthesia.

Three arterioles (n= 1) were found to undergo vasomotion during both the conscious, head-fixed state and isoflurane anesthesia. Power spectral analysis was employed to characterize the differences in frequency of the vasomotor oscillations between experimental conditions (PSD = power spectral density). Vasomotion under isoflurane occurred in two dominant frequencies, including a faster component at ~0.35 Hz. Amplitudes of vasomotor activity was comparable in this representative example (~2-3 μm constriction/dilation from mean diameter).

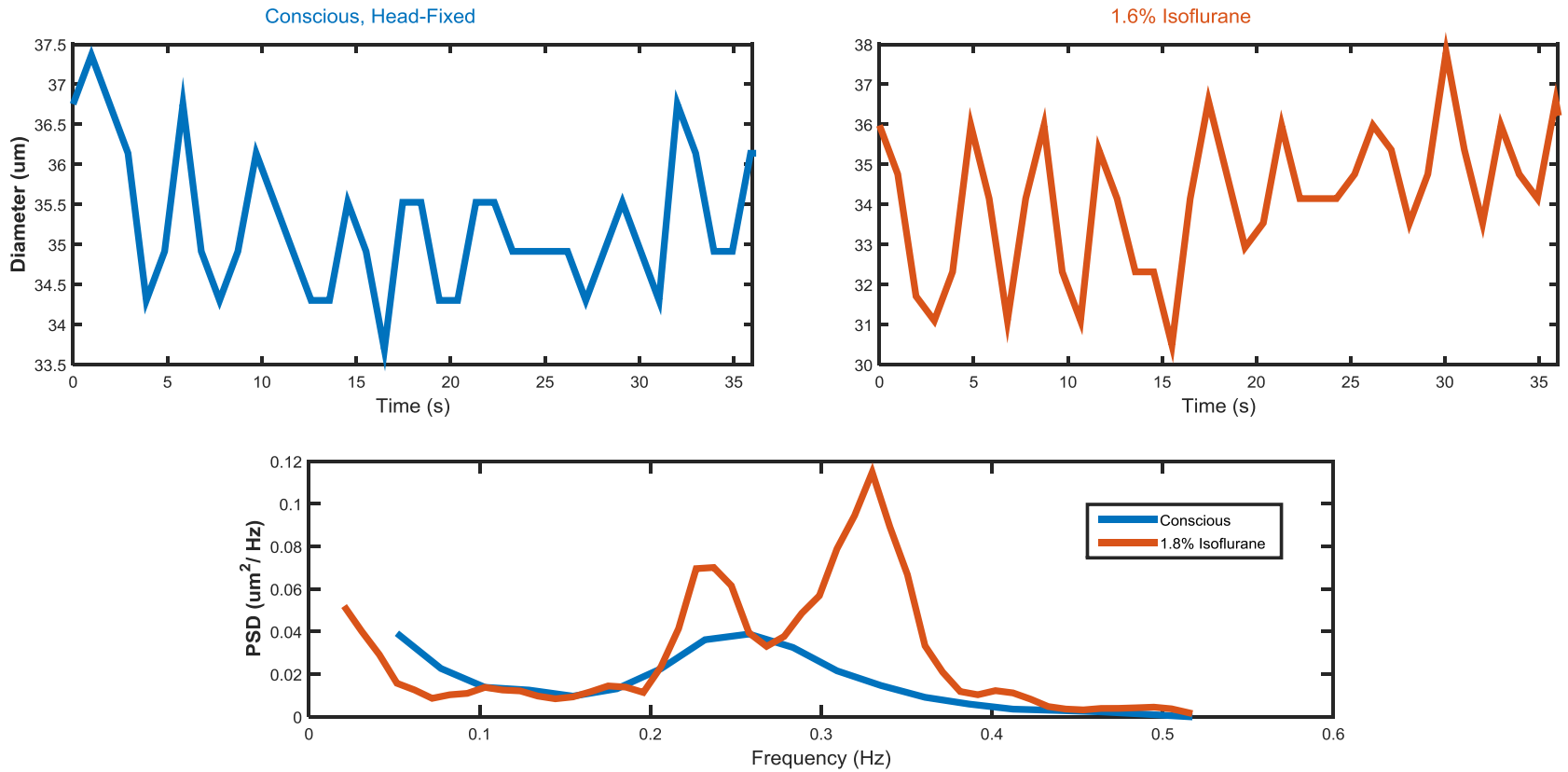
Conscious, Head-Fixed
Diameter (um)
Time (s)
1.6% Isoflurane
Time (s)
PSD (um^2/ Hz)
Frequency (Hz)
Conscious
1.8% Isoflurane

To evaluate the impact of hypertension on arteriolar vasomotion, animals (n=2) subjected to experimental hypertension using ANG-II/salt were imaged daily for 3 days prior to pump implantation, days 3-5 during the intervention period, and 3 days post-pump explantation. Six arterioles were imaged longitudinally during the study period. Prevalence of vasomotion in the basal state was similar to that described above (average prevalence over 3 consecutive basal days). On post-implantation day 3, vasomotion prevalence dropped to 72% and further decreased in the following two days (67% and 39% on day 4 and 5, respectively). Upon explant of the ANG-II osmotic pump and cessation of high salt diet, vasomotion prevalence was restored to near-basal levels (see figure XI).

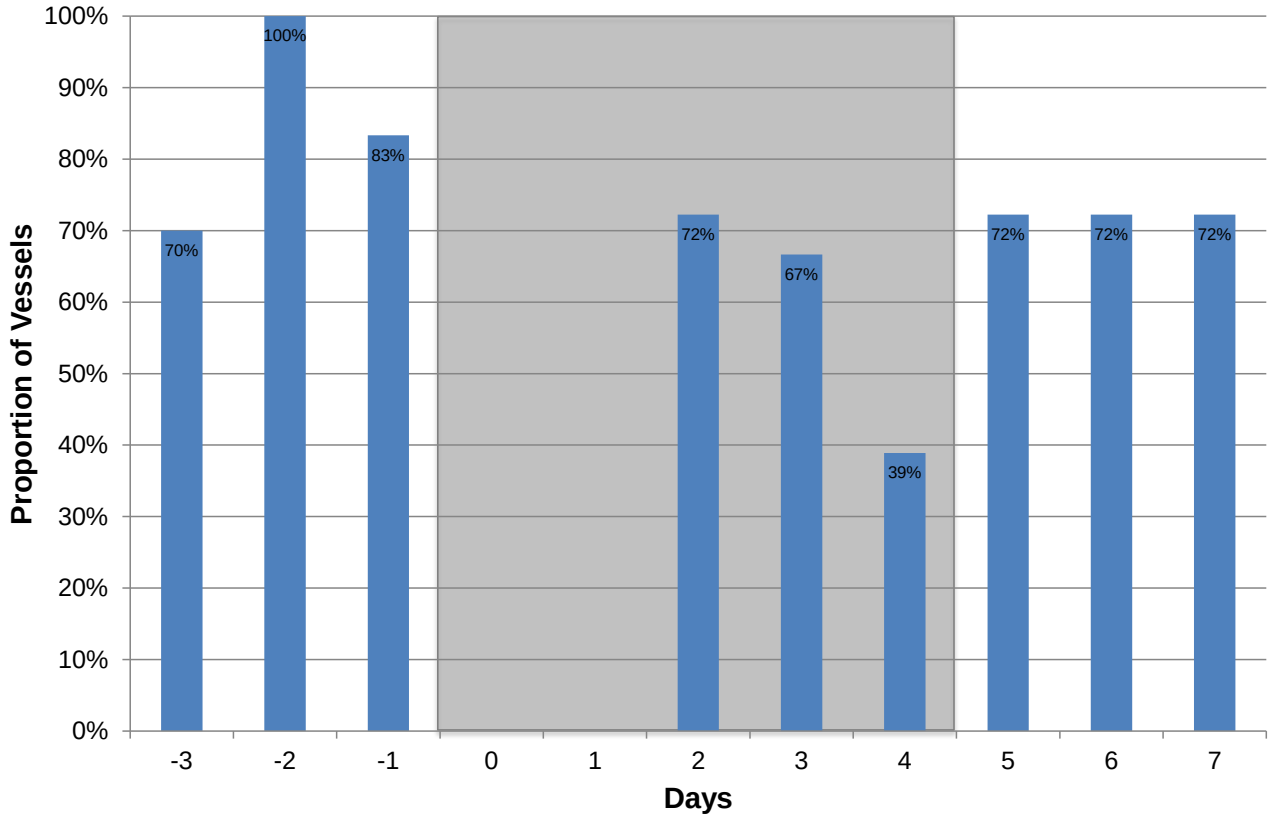

Figure XI – Prevalence of vasomotion during ANG-II/salt hypertension.

Day 0 marks the day of osmotic pump implant and initiation of high salt (6% NaCl) diet. Baseline measurements were obtained on three consecutive days before pump implantation. On days 2-4, a progressive decline in vasomotion prevalence was noted. Removal of the pump restored vasomotion to near-basal levels.

Hexamethonium, a non-depolarizing nicotinic acetylcholine receptor antagonist, was administered to mice (n=4) to assess the role of SNA in arteriolar vasomotion. As most vascular smooth muscle is solely innervated by the sympathetic nervous system, the non-specific ganglionic blockade resulting from hexamethonium is appropriate for this purpose. In 9 paired arterioles, hexamethonium induced a marked vasodilation as compared to the conscious head-fixed state (39.7 ± 2.5 μm to 50.2 ± 2.7 μm, $P = 0.001$). Administration of hexamethonium significantly reduced the prevalence of arteriolar vasomotion (89% to 11% of vessels). In the single arteriole that was undergoing vasomotion post-ganglionic blockade, the vasomotion frequency and amplitude was equivalent to that seen during the conscious, head-fixed state (data not shown). The figure below summarizes the prevalence of vasomotion as measured in all experimental conditions (figure XII).

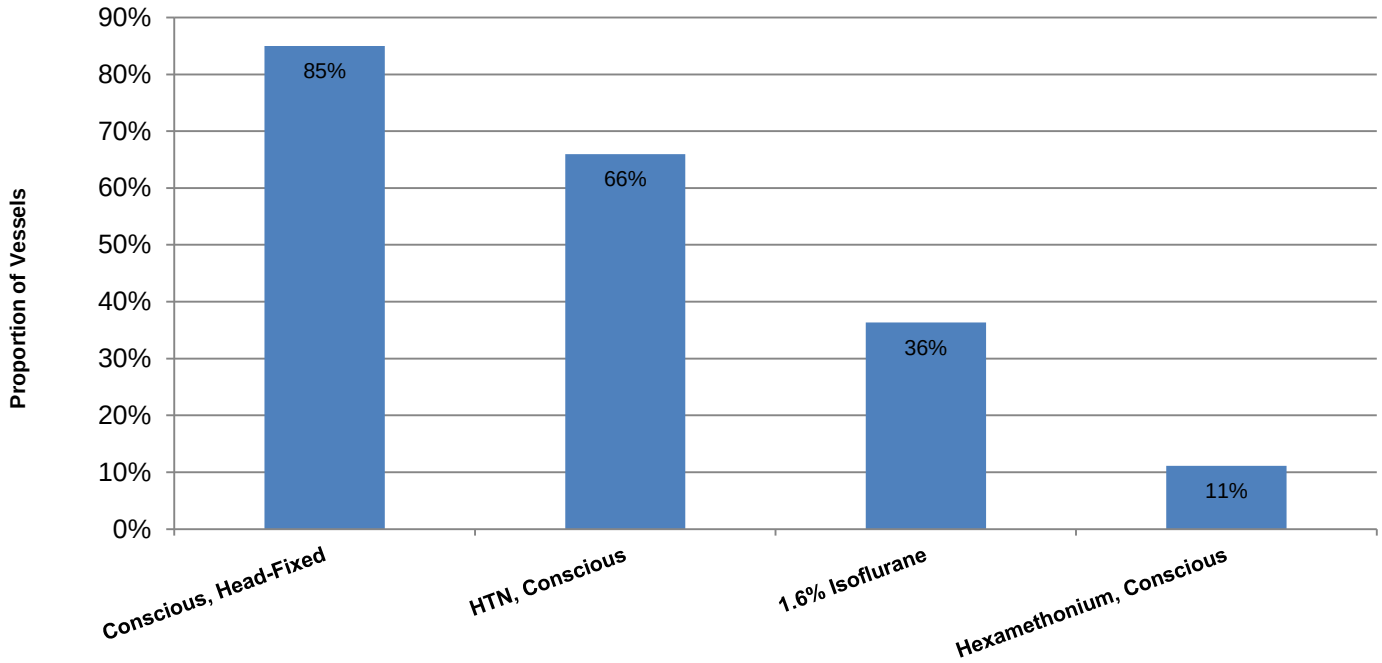

Figure XII – Summary data: prevalence of arteriolar vasomotion.

Graph summarizes the prevalence of vasomotion measured in paired vessels of the peripheral vasculature. Vasomotion was reliably abated upon ganglionic blockade with hexamethonium. 1.6% isoflurane anesthesia also decreased prevalence of vasomotion. Vasomotion in the hypertensive (HTN) state was reported as average across 3 days of serial imaging (for more detail, see figure XI).

3.4) VSM [Ca^{2+}] Measurements

Vasomotion was always associated with spatially homogenous oscillations in VSM cell [Ca^{2+}] (see figure XIII). The arteriole in the example shown below ceased [Ca^{2+}] oscillations ranging from ~400 to 600 nM and dilated 45% in response to isoflurane. As reported previously, maximum [Ca^{2+}] immediately preceded maximal constriction rates for the vessel[2]. This behavior is indicative of similar binding affinity to Ca^{2+} as that of endogenous MLCK[33]. Videos of the vessel under both basal and isoflurane states is available in the supplemental files (supplemental video #2).

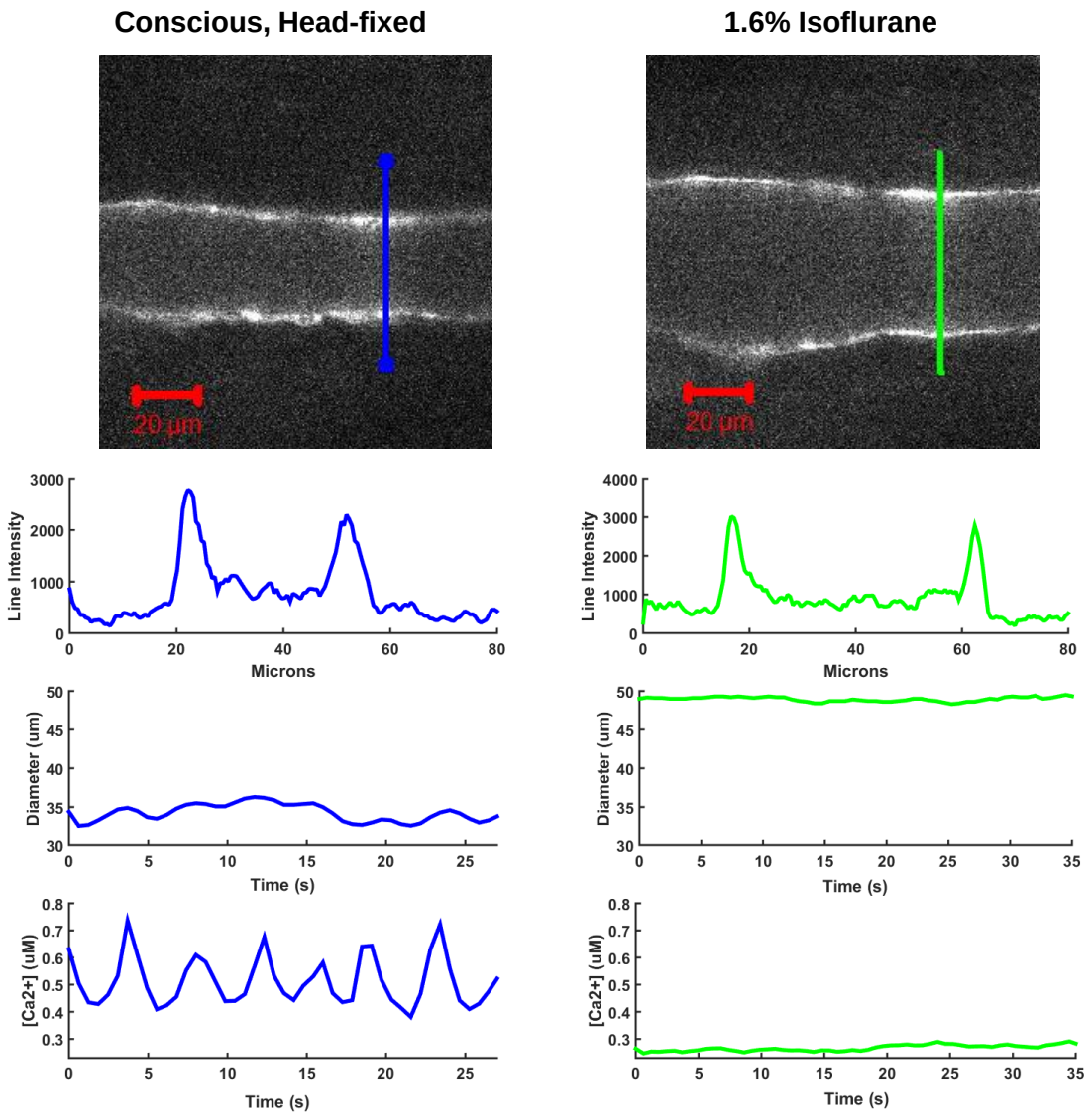

Figure XIII – Measurement of exMLCK arteriolar diameter and [Ca^{2+}] in basal state and under isoflurane anesthesia.

Representative example of [Ca^{2+}] measurements in the same arteriole of conscious, head-fixed (blue trace) and 1.6% isoflurane (green trace) conditions. Custom-made software routines allow for derivation of vessel diameter line intensity profiles generated from self-generated line segments. [Ca^{2+}] was highly synchronized across the vascular wall in the conscious state and was associated with regular oscillatory vasomotion. In this example, the vessel dilated and ceased Ca^{2+} oscillations in response to isoflurane.

Isoflurane anesthesia reduced time-averaged [Ca^{2+}] as compared to the conscious head-fixed state, although statistical significance was not achieved (297 ± 52 nM to 241 ± 20 nM, P = 0.16). [Ca^{2+}] in hypertensive mice subjected to ANG-II/Salt is summarized in the figure below (figure XIV). It should be noted that a calibration experiment was unable to be performed for the optical settings used in acquiring data from the hypertensive animal; the following data is considered close estimations of [Ca^{2+}] based on interpolation of R_{min} and R_{max} values. Basal [Ca^{2+}] of ANG-II/Salt mice was similar to calibrated measurements (305 ± 16 nM) and increased steadily to 652 ± 38 nM on day 4 of hypertension, in agreement with our previous studies[3]. Removal of ANG-II/Salt reduced [Ca^{2+}] to basal levels (285 ± 9 nM).

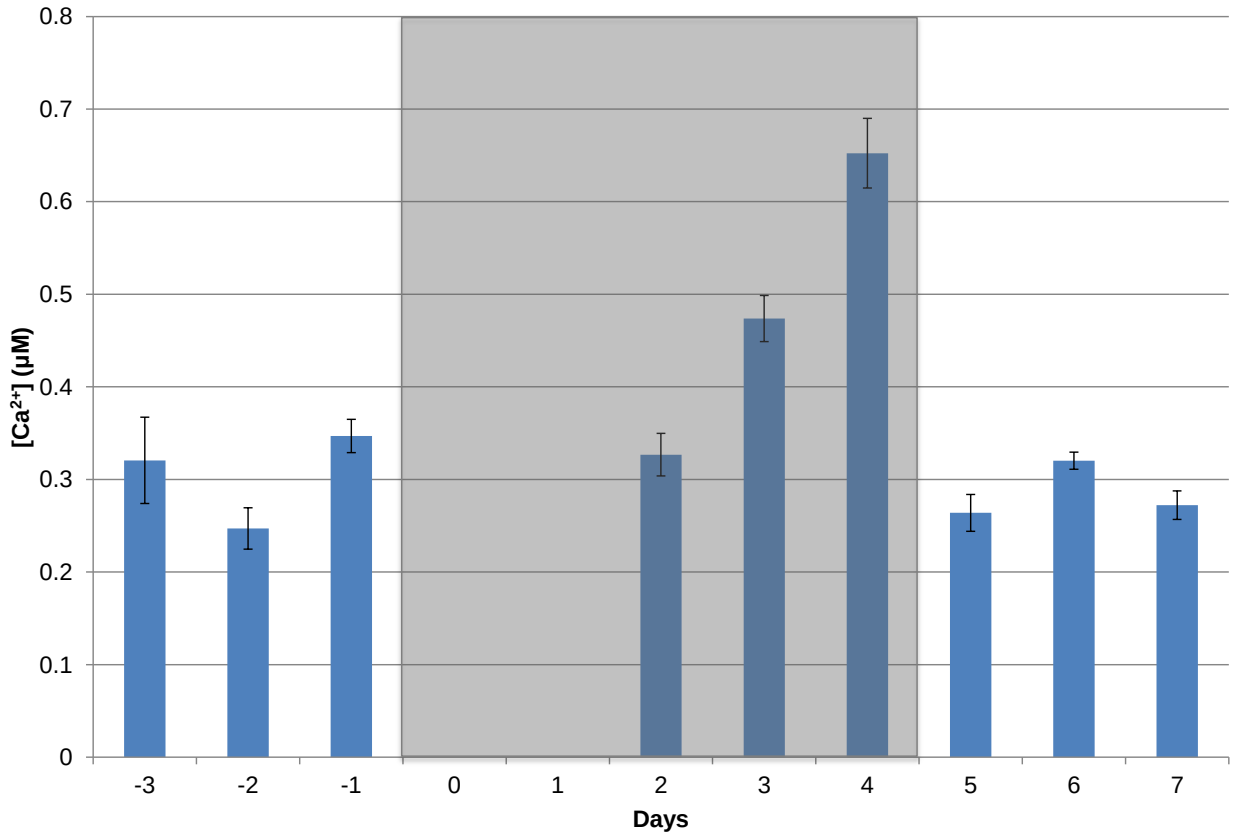

Figure XIV – [Ca^{2+}] changes in arterioles during ANG-II/salt hypertension.

[Ca^{2+}] increased progressively from day 2 to day 4 of ANG-II/salt (from ~300 nM to ~650 nM) and recovered to near-basal levels immediately upon pump explant. The gray area delineates time course of pump implantation.

Hexamethonium strongly terminated Ca^{2+} signaling associated with vasomotion but did not change baseline [Ca^{2+}]. This behavior was reflected in the reduction in time-averaged [Ca^{2+}] from 380 ± 114 nM to 302 ± 47 nM (P = 0.27).

Chapter 4: Discussion

4.1) Methodological Limitations

The methods presented here for measurement of Ca^{2+} signaling events *in vivo* have some limitations. Firstly, serial imaging of the vascular bed under high excitation power elicited significant decline in the signal-to-noise ratio (data not shown). This fact prevented repeated measurements of deep vascular segments ($\geq \sim 70$ μm) in which high excitation power was necessary to excite fluorophores. We speculate that in addition to instability of the biosensor molecule itself, local edema formation due to mechanical damage to the ear during preparation may have led to the noted decline in image quality. In most animals, allowing the animal to recover for 2-3 days without imaging or manipulation of the ear re-established the original optical quality of the preparation. In addition to signal quality concerns, some movement of the conscious animal (and respiratory movement of the anesthetized animal) was transmitted to the ear platform, often creating motion artifacts during image acquisition. The incorporation of the camera to monitor the animal's movements attempted to ameliorate some of these shortcomings, as image acquisition could be synchronized to periods of animal quiescence. In future iterations of our work, the ear immobilization platform design can be refined to prevent motion artifacts that result in decreased signal to noise.

Ideally, quantification of SNA is done with direct recordings of the nerve of interest via bipolar electrode. The invasiveness of this procedure is incompatible with the

desire to measure SNA in the unperturbed physiological environment. In future studies, telemetric means to record SNA could be implemented, as some studies have used such instrumentation to assess SNA in the rabbit[34]. The technology allows for stable nerve recording after postsurgical recovery is complete. Here, limited time and resources prevented the evaluation of these instruments to measure SNA in our study. Instead, non-invasive measure of SNA on the peripheral vasculature was performed via power spectral analysis of arterial blood pressure variability. Blood pressure variability as an index of SNA is not without its limitations, as many examples where known increases in SNA were not associated with changes in LF variability[20]. In the present study, i.p. hydralazine failed to elicit an increase in LF power despite the known baroreflex-mediated increase in vasomotor SNA (data not shown) and we were unable to reproduce results described in the literature[28] (Baudrie *et al*, 2007). It is possible that increased SNA results in tonic constriction (or "fused vasomotion") of some vascular beds, leading to loss of the oscillations in vascular tone that otherwise produce the LF variability (i.e Meyer waves) in blood pressure. More study into the validity of power spectral analysis and the relevance of the LF:HF ratio (as measured by blood pressure variability) as an index of sympatho-vagal interaction is warranted.

4.2) In Vivo Measurements

$[Ca^{2+}]$ measurements in the conscious animal are advantageous in that the arterioles are in a condition closer to physiological than can be achieved in any other condition. We expect cardiovascular control, autonomic nervous system, endothelial, and myogenic mechanisms are as close to the basal state during our imaging experiments.

Previously, our methods involved inhibition of movement via limb restraint. Like the results shown here, this method did not significantly change MAP or HR; however, such restraint is suboptimal. Absence of locomotion precludes the ability of the skeletal muscle pump system to aid in venous return. In addition, restraint may increase hormonal activation of the hypothalamic-pituitary-adrenal axis, leading to increased plasma steroid concentration and modulation of vascular reactivity to vasoactive stimuli like SNA and ANG-II[35, 36]. The crucial result here is that MAP and HR were not altered by the stress induced via head fixation and imaging. This result indicates that our method can allow for studies of vascular physiology or pathophysiology without complications arising from use of isoflurane or conscious restraint. In future studies, a full assessment of vasoactive hormonal substance should be assayed to ensure that the signaling milieu in the animal subjected to head-fixation is comparable to that of the freely moving animal.

To our knowledge, the data presented here represent the first measurement of VSM $[Ca^{2+}]$ in conscious, hypertensive animals with minimal perturbation of the physiological environment. This is attainable due to the non-invasive nature of the methodology. This allows for longitudinal study of VSM Ca^{2+} signaling in the certain blood vessels of a given animal, permitting paired measurements (before and after experimental intervention) and increased statistical power. Because the imaging technique does not involve pain and discomfort for the animal, this procedure can be adapted for study of different vascular beds. One such application allows for study of the cerebral vasculature using a thinned skull or optical cranial window[37], which

could allow for development of models pertinent to stroke, hypertension, and diabetes.

4.3) Vasomotion

Our methodology uniquely allows for assessment of Ca^{2+} signaling in vasomotion, without perturbation from anesthesia or blood vessel exteriorization. Using this method, we sought to evaluate the role of SNA to the ear vasculature in the prevalence of arteriolar vasomotion. Vasomotion of resistance vessels within the ear was much more prevalent in conscious mice than in the anesthetized state, in agreement with an earlier study[2]. In addition, inhibition of SNA by hexamethonium abolished vasomotion in all but one arteriole imaged. It is probable that an incomplete pharmacologic blockade of SNA ensued during the image acquisition of the one vascular segment retaining vasomotion post-hexamethonium. From these results, SNA is clearly an important factor in initiating and/or maintaining vasomotion in the peripheral vascular bed. Stimulation of sympathetic nerve outflow at low frequencies (< 0.2 Hz) via rhythmic electrical discharge of the lumbar sympathetic trunk induces oscillations in blood flow of the same frequency[38]. Interestingly, these frequencies are similar to those reported as ranges of frequencies seen in vasomotion (~0.01 to ~0.3 Hz). Using similar techniques to those presented here, $[Ca^{2+}]$ changes during the vasoconstriction phase of vasomotion has been shown to have similar kinetics to that seen in norepinephrine-mediated spontaneous vasoconstriction[2]. Because of this fact, it is likely that the vasomotion we observed here is the result of norepinephrine (a sympathetic neurotransmitter) acting at the α_1 adrenergic receptor[39].

To our knowledge, the results here represent the first comparative measurements of unperturbed *in situ* VSM [Ca^{2+}] under isoflurane and under ganglionic blockade in conscious animals. Isoflurane, like hexamethonium, strongly reduced the prevalence of arteriolar vasomotion. While the cellular mechanisms of vasomotion have yet to be elucidated, it is likely that voltage-dependent synchronization of sarcoplasmic reticulum Ca^{2+} release and Ca^{2+} entry through voltage dependent channels is necessary for the coordinated changes in [Ca^{2+}] across the VSM[6]. Volatile anesthetics, like isoflurane, have been shown to induce hyperpolarization of *in situ* VSM[40]. As conductance through voltage-dependent Ca^{2+} channels will be attenuated at a hyperpolarized membrane potential, this fact likely partly explains the reduction in vasomotion prevalence under isoflurane anesthesia. Power spectral analysis of MAP under isoflurane anesthesia showed reduction in the low frequency bandwidths associated with sympathetic control, in agreement with previous studies showing attenuation of ganglionic transmission under volatile anesthetic[41]. This attenuation of neural outflow to the vasculature also might explain the reduced vasomotion seen in anesthesia.

Stratification by vessel diameter in the conscious head-fixed state did not elicit any predictable vessel responses upon administration of anesthesia. To that end, it is unclear what specific effects isoflurane has on VSM. *In vitro,* volatile anesthetics are shown to both augment and attenuate endothelium-derived nitric oxide production and inhibit endothelium-derived hyperpolarizing factor[40]. It is possible that variable

responses to isoflurane were mediated by non-neural control of vascular tone, resulting in vasoconstriction or dilation. In our studies, mice maintained on isoflurane anesthesia show a further reduction in MAP when subjected to i.p hexamethonium, suggesting that SNA is further attenuated by ganglionic blockade and the abolition of SNA is not complete under isoflurane (data not shown). Because of the confounding nature of effects of isoflurane on the VSM and its neural control, it is difficult to interpret the direct effects of anesthesia on arteriolar vasomotion. In the case of the one animal exhibiting vasomotion under anesthesia, it is possible that SNA to the VSM of the peripheral vasculature was increased above a threshold level for maintenance of vasomotion. Indeed, volatile anesthetics have been shown to increase SNA to the skeletal muscle in healthy humans mediated via the arterial baroreflex[42]. In addition, bronchial irritation can induce augmentation of SNA, which may explain the presence of vasomotion in the one animal.

Prevalence of vasomotion in sub-acutely hypertensive animals progressively decreased from day 3 to day 5 of ANG-II/salt intervention. In the same treatment in previous work in our lab, MAP increased by 26 mmHg on average during this time. We hypothesize that the reduction in vasomotion across the ear vasculature is mediated by a baroreceptor-mediated decrease in SNA. Blood pressure variability, as measured with non-parametric power spectral analysis corroborates this hypothesis, as LF power and the LF:HF power ratio progressively decreases through day 4 of ANG-II/salt experimental hypertension. This finding is contrary to previous studies of heart rate variability; in human patients with essential hypertension, LF power was

found to be significantly higher as compared to normotensive controls. [43] In addition, infusions of ANG-II administered simultaneously with a low salt diet have been shown to exhibit augmentations in global vasomotor SNA as measured by depressor response to ganglionic blockade, however MAP was not significantly elevated[44]. The pertinence of these findings to our study here is convoluted, as organ-specific increases in SNA has been implicated in this form of experimental hypertension[20]. For example, ANG-II/salt hypertension has been shown to differentially increase SNA to the mesenteric vascular bed while maintaining renal and skeletal muscle SNA[45]. In addition, celiac ganglionectomy was shown to attenuate MAP changes in response to ANG-II/salt[46]. Thus, it is clear that regionally specific changes of SNA occur in ANG-II/salt-induced hypertension. Ensuing research should seek to characterize the SNA changes to ANG-II in the peripheral vasculature, like the ear vasculature examined here.

The mechanistic understanding of vasomotion and elucidation of its physiological role is crucial, as pathological states and common clinical interventions (like anesthesia and pharmacology) have been shown to modulate its prevalence and behavior *in vivo*. While unconfirmed, arteriolar vasomotion likely enhances tissue dialysis[7, 21]. Thus, our evidence for the essential role of SNA in the appearance of arteriolar vasomotion *in vivo* has several important implications. Because arteriolar vasomotion is highly present in the unadulterated condition, administration of volatile anesthesia may compromise dialysis of the periphery, possibly resulting in uncharacterized cellular damage. If vasomotion is strongly linked to sympathetic

nervous control of a particular vascular segment, the phenomena could possibly be used as a surrogate marker for evaluation of level of vascular sympathetic outflow. Indeed, several groups have suggested that reduced arterial vasomotion could be an early index of sympathetic dysfunction[47, 48].

Further investigation is warranted to fully characterize the cellular basis of vasomotion. As novel genetically encoded biosensors are developed and mouse strains are made available, our method of imaging presented here can allow for non-invasive investigation of vascular physiology with all control mechanisms intact and operating at a basal state. To further elucidate the cellular means of oscillatory vasomotion, newly developed membrane potential-sensitive proteins (e.g Mermaid, VSFP2.4) could be employed. These second-generation protein-based fluorescent voltage sensors are ratiometric FRET-based indicators that exhibit a sizable dynamic range (-100 mV to 0 mV) and ratio change with temporal activation characteristics compatible with such an application[49]. The next steps to evaluate the role of SNA in vasomotion should implement such proteins to elucidate the characteristics of voltage-dependent synchronization of Ca^{2+} release in VSM. In addition, pharmacological means to increase SNA to the peripheral ear could be administered to determine changes in arteriolar vasomotion. Vasodilatory drugs, like the K^+ channel conductance augmenter hydralazine, cause a baroreflex-mediated increase in global vasomotor SNA as measured by power spectral analysis[28]. If our hypothesis holds, increase in SNA to the peripheral vasculature should be accompanied by an increase in vasomotion prevalence.

The results gleaned here from modulation of SNA in the mouse are directly applicable to human cardiovascular control mechanisms. It is well known that sympathetic nerve bursting rates are slower in humans than in small animals (rodents, sheep, rabbit), although the timing of the bursts with respect to the cardiac cycle are consistent between species[20]. In the power spectral analysis of blood pressure variability, this change is reflected by different bandwidths attributed to SNA and vagal control; in humans, the LF component attributed to sympathetic control of the cardiovascular system is defined as 0.07- 0.15 Hz[45]. Interestingly, this bandwidth includes many frequencies at which cutaneous vasomotion is measured in humans[7]. As mentioned above (see ***Introduction***), diabetic patients exhibit impaired vasomotion as compared to healthy patients. This vasomotion occurs at 0.1 Hz and could potentially be driven by altered levels of tonic SNA that discharges at a similar frequency. Thus, because of the correlations to human data describing slower rates of vascular SNA bursting, we believe the murine model is applicable for the study of SNA and how it correlates to the prevalence of arteriolar vasomotion.

Bibliography

1. Wier WG. More in vivo experimentation is needed in cardiovascular physiology. *Am J Physiol Heart Circ Physiol*. 2014;307:H121-3.

2. Fairfax ST, Mauban JR, Hao S, Rizzo MA, Zhang J, Wier WG. Ca^{2+} signaling in arterioles and small arteries of conscious, restrained, optical biosensor mice. *Front Physiol*. 2014;5:387.

3. Mauban JR, Fairfax ST, Rizzo MA, Zhang J, Wier WG. A method for noninvasive longitudinal measurements of [Ca^{2+}] in arterioles of hypertensive optical biosensor mice. *Am J Physiol Heart Circ Physiol*. 2014;307:H173-81.

4. Mauban JR, Zacharia J, Zhang J, Wier WG. Vascular tone and Ca(2+) signaling in murine cremaster muscle arterioles in vivo. *Microcirculation*. 2013;20:269-277.

5. Wang Y, Chen L, Wier WG, Zhang J. Intravital Förster resonance energy transfer imaging reveals elevated [Ca^{2+}]$_i$ and enhanced sympathetic tone in femoral arteries of angiotensin II-infused hypertensive biosensor mice. *J Physiol*. 2013;591:5321-5336.

6. Aalkjaer C, Nilsson H. Vasomotion: cellular background for the oscillator and for the synchronization of smooth muscle cells. *Br J Pharmacol*. 2005;144:605-616.

7. Aalkjaer C, Boedtkjer D, Matchkov V. Vasomotion - what is currently thought? *Acta Physiol (Oxf)*. 2011;202:253-269.

8. Mauban JR, Lamont C, Balke CW, Wier WG. Adrenergic stimulation of rat resistance arteries affects Ca^{2+} sparks, Ca^{2+} waves, and Ca^{2+} oscillations. *Am J Physiol Heart Circ Physiol*. 2001;280:H2399-405.

9. Peng H, Matchkov V, Ivarsen A, Aalkjaer C, Nilsson H. Hypothesis for the initiation of vasomotion. *Circ Res*. 2001;88:810-815.

10. Mauban JR, Wier WG. Essential role of EDHF in the initiation and maintenance of adrenergic vasomotion in rat mesenteric arteries. *Am J Physiol Heart Circ Physiol*. 2004;287:H608-16.

11. Sakurai T, Terui N. Effects of sympathetically induced vasomotion on tissue-capillary fluid exchange. *Am J Physiol Heart Circ Physiol*. 2006;291:H1761-7.

12. Meyer C, de Vries G, Davidge ST, Mayes DC. Reassessing the mathematical modeling of the contribution of vasomotion to vascular resistance. *J Appl Physiol (1985)*. 2002;92:888-889.

13. Kislukhin VV. Stochasticity of flow through microcirculation as a regulator of oxygen delivery. *Theor Biol Med Model*. 2010;7:29-4682-7-29.

14. Pradhan RK, Chakravarthy VS, Prabhakar A. Effect of chaotic vasomotion in skeletal muscle on tissue oxygenation. *Microvasc Res*. 2007;74:51-64.

15. Hapuarachchi T, Park CS, Payne S. Quantification of the effects of vasomotion on mass transport to tissue from axisymmetric blood vessels. *J Theor Biol*. 2010;264:553-559.

16. Schmidt JA, Intaglietta M, Borgstrom P. Periodic hemodynamics in skeletal muscle during local arterial pressure reduction. *J Appl Physiol (1985)*. 1992;73:1077-1083.

17. Bertuglia S, Colantuoni A, Coppini G, Intaglietta M. Hypoxia- or hyperoxia-induced changes in arteriolar vasomotion in skeletal muscle microcirculation. *Am J Physiol*. 1991;260:H362-72.

18. Osol G, Halpern W. Spontaneous vasomotion in pressurized cerebral arteries from genetically hypertensive rats. *Am J Physiol*. 1988;254:H28-33.

19. Schmidt C, Adechokan S, Mouhli J. Laser-Doppler flowmetry and arterial diseases of the limbs. Correlations with measurement of transcutaneous oxygen pressure. *J Mal Vasc*. 1996;21:294-298.

20. Malpas SC. Sympathetic nervous system overactivity and its role in the development of cardiovascular disease. *Physiol Rev*. 2010;90:513-557.

21. Bocchi L, Evangelisti A, Barrella M, Scatizzi L, Bevilacqua M. Recovery of 0.1Hz microvascular skin blood flow in dysautonomic diabetic (type 2) neuropathy by using Frequency Rhythmic Electrical Modulation System (FREMS). *Med Eng Phys*. 2010;32:407-413.

22. Isotani E, Zhi G, Lau KS, et al. Real-time evaluation of myosin light chain kinase activation in smooth muscle tissues from a transgenic calmodulin-biosensor mouse. *Proc Natl Acad Sci U S A*. 2004;101:6279-6284.

23. Tallini YN, Ohkura M, Choi BR, et al. Imaging cellular signals in the heart in vivo: Cardiac expression of the high-signal Ca^{2+} indicator GCaMP2. *Proc Natl Acad Sci U S A*. 2006;103:4753-4758.

24. Tallini YN, Brekke JF, Shui B, et al. Propagated endothelial Ca^{2+} waves and arteriolar dilation in vivo: measurements in Cx40BAC GCaMP2 transgenic mice. *Circ Res*. 2007;101:1300-1309.

25. Xin HB, Deng KY, Rishniw M, Ji G, Kotlikoff MI. Smooth muscle expression of Cre recombinase and eGFP in transgenic mice. *Physiol Genomics*. 2002;10:211-215.

26. Huang S, Heikal AA, Webb WW. Two-photon fluorescence spectroscopy and microscopy of NAD(P)H and flavoprotein. *Biophys J*. 2002;82:2811-2825.

27. Boudreau E, Chen G, Li X, Buck K, Hitzemann R, Hickman D. Intraperitoneal catheter placement for pharmacological imaging studies in conscious mice. *Lab Anim (NY)*. 2010;39:23-25.

28. Baudrie V, Laude D, Elghozi JL. Optimal frequency ranges for extracting information on cardiovascular autonomic control from the blood pressure and pulse interval spectrograms in mice. *Am J Physiol Regul Integr Comp Physiol*. 2007;292:R904-12.

29. Stauss HM. Identification of blood pressure control mechanisms by power spectral analysis. *Clin Exp Pharmacol Physiol*. 2007;34:362-368.

30. Pagani M, Lombardi F, Guzzetti S, et al. Power spectral analysis of heart rate and arterial pressure variabilities as a marker of sympatho-vagal interaction in man and conscious dog. *Circ Res*. 1986;59:178-193.

31. Fazan R,Jr, Huber DA, Silva CA, Dias da Silva VJ, Salgado MC, Salgado HC. Sildenafil acts on the central nervous system increasing sympathetic activity. *J Appl Physiol (1985)*. 2008;104:1683-1689.

32. Pagani M, Montano N, Porta A, et al. Relationship between spectral components of cardiovascular variabilities and direct measures of muscle sympathetic nerve activity in humans. *Circulation*. 1997;95:1441-1448.

33. Hong F, Haldeman BD, John OA, et al. Characterization of tightly associated smooth muscle myosin-myosin light-chain kinase-calmodulin complexes. *J Mol Biol*. 2009;390:879-892.

34. Malpas SC, Ramchandra R, Guild SJ, Budgett DM, Barrett CJ. Baroreflex mechanisms regulating mean level of SNA differ from those regulating the timing and entrainment of the sympathetic discharges in rabbits. *Am J Physiol Regul Integr Comp Physiol*. 2006;291:R400-9.

35. Malisch JL, Saltzman W, Gomes FR, Rezende EL, Jeske DR, Garland T,Jr. Baseline and stress-induced plasma corticosterone concentrations of mice selectively bred for high voluntary wheel running. *Physiol Biochem Zool*. 2007;80:146-156.

36. Ullian ME. The role of corticosteriods in the regulation of vascular tone. *Cardiovasc Res*. 1999;41:55-64.

37. Drew PJ, Shih AY, Driscoll JD, et al. Chronic optical access through a polished and reinforced thinned skull. *Nat Methods*. 2010;7:981-984.

38. Stauss HM, Stegmann JU, Persson PB, Habler HJ. Frequency response characteristics of sympathetic transmission to skin vascular smooth muscles in rats. *Am J Physiol*. 1999;277:R591-600.

39. Zacharia J, Mauban JR, Raina H, Fisher SA, Wier WG. High vascular tone of mouse femoral arteries in vivo is determined by sympathetic nerve activity via alpha1A- and alpha1D-adrenoceptor subtypes. *PLoS One*. 2013;8:e65969.

40. Yamazaki M, Stekiel TA, Bosnjak ZJ, Kampine JP, Stekiel WJ. Effects of volatile anesthetic agents on in situ vascular smooth muscle transmembrane potential in resistance- and capacitance-regulating blood vessels. *Anesthesiology*. 1998;88:1085-1095.

41. Boban N, McCallum JB, Schedewie HK, Boban M, Kampine JP, Bosnjak ZJ. Direct comparative effects of isoflurane and desflurane on sympathetic ganglionic transmission. *Anesth Analg*. 1995;80:127-134.

42. Ebert TJ, Muzi M. Sympathetic hyperactivity during desflurane anesthesia in healthy volunteers. A comparison with isoflurane. *Anesthesiology*. 1993;79:444-453.

43. Guzzetti S, Piccaluga E, Casati R, et al. Sympathetic predominance in essential hypertension: a study employing spectral analysis of heart rate variability. *J Hypertens*. 1988;6:711-717.

44. McBryde FD, Guild SJ, Barrett CJ, Osborn JW, Malpas SC. Angiotensin II-based hypertension and the sympathetic nervous system: the role of dose and increased dietary salt in rabbits. *Exp Physiol*. 2007;92:831-840.

45. Kuroki MT, Guzman PA, Fink GD, Osborn JW. Time-dependent changes in autonomic control of splanchnic vascular resistance and heart rate in ANG II-salt hypertension. *Am J Physiol Heart Circ Physiol*. 2012;302:H763-9.

46. King AJ, Osborn JW, Fink GD. Splanchnic circulation is a critical neural target in angiotensin II salt hypertension in rats. *Hypertension*. 2007;50:547-556.

47. Meyer MF, Rose CJ, Hulsmann JO, Schatz H, Pfohl M. Impaired 0.1-Hz vasomotion assessed by laser Doppler anemometry as an early index of peripheral sympathetic neuropathy in diabetes. *Microvasc Res*. 2003;65:88-95.

48. Bernardi L, Rossi M, Leuzzi S, et al. Reduction of 0.1 Hz microcirculatory fluctuations as evidence of sympathetic dysfunction in insulin-dependent diabetes. *Cardiovasc Res*. 1997;34:185-191.

49. Patti J, Isacoff EY. Measuring membrane voltage with fluorescent proteins. *Cold Spring Harb Protoc*. 2013;2013:606-613.